asbestos-induced signaling pathways, the precise role of individual MMPs in asbestos-induced lung pathologies will be explored in the future by using MMP12 and MMP13 knockout models. FJ

This work was supported by National Institutes of Health Grant PO1HL67004. Dr. Pamela Vacek (Department of Medical Biostatistics, University of Vermont, Burlington, VT) assisted in the statistical analyses. We also wish to acknowledge Scott Tighe and Timothy Hunter from the Vermont Cancer Center DNA Analysis Facility at the University of Vermont for performing oligonucleotide microarrays with the provided RNA samples. Oligonucleotide microarrays and real-time quantitative polymerase chain reactions were performed in the VT Cancer Center DNA Analysis Facility and were supported in part by grant P30CA22435 from the NCI. The views expressed are those of author and do not represent the views of the NCI.

REFERENCES

1. Mossman, B. T., and Churg, A. (1998) Mechanisms in the pathogenesis of asbestosis and silicosis. *Am. J. Respir. Crit. Care Med.* **157,** 1666–1680
2. Mossman, B. T., and Gee, J. B. (1989) Asbestos-related diseases. *N. Engl. J. Med.* **320,** 1721–1730
3. Mossman, B. T., Marsh, J. P., Sesko, A., Hill, S., Shatos, M. A., Doherty, J., Petruska, J., Adler, K. B., Hemenway, D., Mickey, R., and et al. (1990) Inhibition of lung injury, inflammation, and interstitial pulmonary fibrosis by polyethylene glycol-conjugated catalase in a rapid inhalation model of asbestosis. *Am. Rev. Respir. Dis.* **141,** 1266–1271
4. Shukla, A., Gulumian, M., Hei, T. K., Kamp, D., Rahman, Q., and Mossman, B. T. (2003) Multiple roles of oxidants in the pathogenesis of asbestos-induced diseases. *Free Radic. Biol. Med.* **34,** 1117–1129
5. Winkler, M. K., and Fowlkes, J. L. (2002) Metalloproteinase and growth factor interactions: do they play a role in pulmonary fibrosis? *Am. J. Physiol. Lung Cell Mol. Physiol.* **283,** L1–11
6. Shapiro, S. D. (1999) Diverse roles of macrophage matrix metalloproteinases in tissue destruction and tumor growth. *Thromb. Haemost.* **82,** 846–849
7. Shapiro, S. D., and Senior, R. M. (1999) Matrix metalloproteinases. Matrix degradation and more. *Am. J. Respir. Cell Mol. Biol.* **20,** 1100–1102
8. Hayashi, T., Stetler-Stevenson, W. G., Fleming, M. V., Fishback, N., Koss, M. N., Liotta, L. A., Ferrans, V. J., and Travis, W. D. (1996) Immunohistochemical study of metalloproteinases and their tissue inhibitors in the lungs of patients with diffuse alveolar damage and idiopathic pulmonary fibrosis. *Am. J. Pathol.* **149,** 1241–1256
9. Selman, M., Ruiz, V., Cabrera, S., Segura, L., Ramirez, R., Barrios, R., and Pardo, A. (2000) TIMP-1, -2, -3, and -4 in idiopathic pulmonary fibrosis. A prevailing nondegradative lung microenvironment? *Am. J. Physiol. Lung Cell Mol. Physiol.* **279,** L562–574
10. Zuo, F., Kaminski, N., Eugui, E., Allard, J., Yakhini, Z., Ben-Dor, A., Lollini, L., Morris, D., Kim, Y., DeLustro, B., Sheppard, D., Pardo, A., Selman, M., and Heller, R. A. (2002) Gene expression analysis reveals matrilysin as a key regulator of pulmonary fibrosis in mice and humans. *Proc. Natl. Acad. Sci. U.S.A.* **99,** 6292–6297
11. Stamenkovic, I. (2000) Matrix metalloproteinases in tumor invasion and metastasis. *Semin. Cancer Biol.* **10,** 415–433
12. Vu, T. H., and Werb, Z. (2000) Matrix metalloproteinases: effectors of development and normal physiology. *Genes Dev.* **14,** 2123–2133
13. Werb, Z. (1997) ECM and cell surface proteolysis: regulating cellular ecology. *Cell* **91,** 439–442
14. Lounsbury, K. M., Stern, M., Taatjes, D., Jaken, S., and Mossman, B. T. (2002) Increased localization and substrate activation of protein kinase C delta in lung epithelial cells following exposure to asbestos. *Am. J. Pathol.* **160,** 1991–2000
15. Shukla, A., Stern, M., Lounsbury, K. M., Flanders, T., and Mossman, B. T. (2003) Asbestos-induced apoptosis is protein kinase C delta-dependent. *Am. J. Respir. Cell Mol. Biol.* **29,** 198–205
16. Robledo, R. F., Buder-Hoffmann, S. A., Cummins, A. B., Walsh, E. S., Taatjes, D. J., and Mossman, B. T. (2000) Increased phosphorylated extracellular signal-regulated kinase immunoreactivity associated with proliferative and morphologic lung alterations after chrysotile asbestos inhalation in mice. *Am. J. Pathol.* **156,** 1307–1316
17. Miyamoto, A., Nakayama, K., Imaki, H., Hirose, S., Jiang, Y., Abe, M., Tsukiyama, T., Nagahama, H., Ohno, S., Hatakeyama, S., and Nakayama, K. I. (2002) Increased proliferation of B cells and auto-immunity in mice lacking protein kinase Cdelta. *Nature* **416,** 865–869
18. Malkinson, A. M., Dwyer-Nield, L. D., Rice, P. L., and Dinsdale, D. (1997) Mouse lung epithelial cell lines–tools for the study of differentiation and the neoplastic phenotype. *Toxicology* **123,** 53–100
19. Gschwendt, M., Muller, H. J., Kielbassa, K., Zang, R., Kittstein, W., Rincke, G., and Marks, F. (1994) Rottlerin, a novel protein kinase inhibitor. *Biochem. Biophys. Res. Commun.* **199,** 93–98
20. Zanella, C. L., Posada, J., Tritton, T. R., and Mossman, B. T. (1996) Asbestos causes stimulation of the extracellular signal-regulated kinase 1 mitogen-activated protein kinase cascade after phosphorylation of the epidermal growth factor receptor. *Cancer Res.* **56,** 5334–5338
21. Muscella, A., Elia, M. G., Greco, S., Storelli, C., and Marsigliante, S. (2003) Activation of P2Y2 receptor induces c-FOS protein through a pathway involving mitogen-activated protein kinases and phosphoinositide 3-kinases in HeLa cells. *J. Cell. Physiol.* **195,** 234–240
22. Burch, P. M., Yuan, Z., Loonen, A., and Heintz, N. H. (2004) An extracellular signal-regulated kinase 1- and 2-dependent program of chromatin trafficking of c-Fos and Fra-1 is required for cyclin D1 expression during cell cycle reentry. *Mol. Cell. Biol.* **24,** 4696–4709
23. Zhang, Q., Adiseshaiah, P., and Reddy, S. P. (2005) Matrix metalloproteinase/epidermal growth factor receptor/mitogen-activated protein kinase signaling regulate fra-1 induction by cigarette smoke in lung epithelial cells. *Am. J. Respir. Cell Mol. Biol.* **32,** 72–81
24. Wylie, A. G., Skinner, H. C., Marsh, J., Snyder, H., Garzione, C., Hodkinson, D., Winters, R., and Mossman, B. T. (1997) Mineralogical features associated with cytotoxic and proliferative effects of fibrous talc and asbestos on rodent tracheal epithelial and pleural mesothelial cells. *Toxicol. Appl. Pharmacol.* **147,** 143–150
25. Shukla, A., Timblin, C., BeruBe, K., Gordon, T., McKinney, W., Driscoll, K., Vacek, P., and Mossman, B. T. (2000) Inhaled particulate matter causes expression of nuclear factor (NF)-kappaB-related genes and oxidant-dependent NF-kappaB activation in vitro. *Am. J. Respir. Cell Mol. Biol.* **23,** 182–187
26. Shipley, J. M., Wesselschmidt, R. L., Kobayashi, D. K., Ley, T. J., and Shapiro, S. D. (1996) Metalloelastase is required for macrophage-mediated proteolysis and matrix invasion in mice. *Proc. Natl. Acad. Sci. U.S.A.* **93,** 3942–3946
27. Sabo-Attwood, T., Ramos-Nino, M., Bond, J., Butnor, K. J., Heintz, N., Gruber, A. D., Steele, C., Taatjes, D. J., Vacek, P., and Mossman, B. T. (2005) Gene Expression Profiles Reveal Increased mClca3 (Gob5) Expression and Mucin Production in a Murine Model of Asbestos-Induced Fibrogenesis. *Am. J. Pathol.* **167,** 1243–1256
28. Shukla, A., Gell, J., Barrett, T. F., MacPherson M., Butnor, K., Hube, S., Rincon, M., Devis, J., Lounsbury, K., and Mossman, B. T. (2005) Decreased asbestos-induced pulmonary fibrosis in PKC delta knockout mice, a possible result of altered inflammatory profiles. *FASEB J.* **19,** A491
29. Scapoli, L., Ramos-Nino, M. E., Martinelli, M., and Mossman, B. T. (2004) Src-dependent ERK5 and Src/EGFR-dependent ERK1/2 activation is required for cell proliferation by asbestos. *Oncogene* **23,** 805–813
30. Fukuda, Y., Ishizaki, M., Kudoh, S., Kitaichi, M., and Yamanaka, N. (1998) Localization of matrix metalloproteinases-1, -2, and -9

and tissue inhibitor of metalloproteinase-2 in interstitial lung diseases. *Lab. Invest.* **78,** 687–698
31. Lemjabbar, H., Gosset, P., Lechapt-Zalcman, E., Franco-Montoya, M. L., Wallaert, B., Harf, A., and Lafuma, C. (1999) Overexpression of alveolar macrophage gelatinase B (MMP-9) in patients with idiopathic pulmonary fibrosis: effects of steroid and immunosuppressive treatment. *Am. J. Respir. Cell Mol. Biol.* **20,** 903–913
32. Corbel, M., Caulet-Maugendre, S., Germain, N., Molet, S., Lagente, V., and Boichot, E. (2001) Inhibition of bleomycin-induced pulmonary fibrosis in mice by the matrix metalloproteinase inhibitor batimastat. *J. Pathol.* **193,** 538–545
33. Perez-Ramos, J., de Lourdes Segura-Valdez, M., Vanda, B., Selman, M., and Pardo, A. (1999) Matrix metalloproteinases 2, 9, and 13, and tissue inhibitors of metalloproteinases 1 and 2 in experimental lung silicosis. *Am. J. Respir. Crit. Care Med.* **160,** 1274–1282
34. Ortiz, L. A., Lasky, J., Gozal, E., Ruiz, V., Lungarella, G., Cavarra, E., Brody, A. R., Friedman, M., Pardo, A., and Selman, M. (2001) Tumor necrosis factor receptor deficiency alters matrix metalloproteinase 13/tissue inhibitor of metalloproteinase 1 expression in murine silicosis. *Am. J. Respir. Crit. Care Med.* **163,** 244–252
35. Shapiro, S. D., Griffin, G. L., Gilbert, D. J., Jenkins, N. A., Copeland, N. G., Welgus, H. G., Senior, R. M., and Ley, T. J. (1992) Molecular cloning, chromosomal localization, and bacterial expression of a murine macrophage metalloelastase. *J. Biol. Chem.* **267,** 4664–4671
36. Shapiro, S. D., Kobayashi, D. K., and Ley, T. J. (1993) Cloning and characterization of a unique elastolytic metalloproteinase produced by human alveolar macrophages. *J. Biol. Chem.* **268,** 23824–23829
37. Lavigne, M. C., and Eppihimer, M. J. (2005) Cigarette smoke condensate induces MMP-12 gene expression in airway-like epithelia. *Biochem. Biophys. Res. Commun.* **330,** 194–203
38. Vincenti, M. P. (2001) The matrix metalloproteinase (MMP) and tissue inhibitor of metalloproteinase (TIMP) genes. Transcriptional and posttranscriptional regulation, signal transduction and cell-type-specific expression. *Methods Mol. Biol.* **151,** 121–148
39. Rao, J. S. (2003) Molecular mechanisms of glioma invasiveness: the role of proteases. *Nat. Rev. Cancer* **3,** 489–501
40. Westermarck, J., and Kahari, V. M. (1999) Regulation of matrix metalloproteinase expression in tumor invasion. *FASEB J.* **13,** 781–792
41. Shukla, A., Timblin, C. R., Hubbard, A. K., Bravman, J., and Mossman, B. T. (2001) Silica-induced activation of c-Jun-NH2-terminal amino kinases, protracted expression of the activator protein-1 proto-oncogene, fra-1, and S-phase alterations are mediated via oxidative stress. *Cancer Res.* **61,** 1791–1795
42. Shum, J. K., Melendez, J. A., and Jeffrey, J. J. (2002) Serotonin-induced MMP-13 production is mediated via phospholipase C, protein kinase C, and ERK1/2 in rat uterine smooth muscle cells. *J. Biol. Chem.* **277,** 42830–42840
43. Woo, J. H., Lim, J. H., Kim, Y. H., Suh, S. I., Min do, S., Chang, J. S., Lee, Y. H., Park, J. W., and Kwon, T. K. (2004) Resveratrol inhibits phorbol myristate acetate-induced matrix metalloproteinase-9 expression by inhibiting JNK and PKC delta signal transduction. *Oncogene* **23,** 1845–1853
44. Ellerbroek, S. M., Halbleib, J. M., Benavidez, M., Warmka, J. K., Wattenberg, E. V., Stack, M. S., and Hudson, L. G. (2001) Phosphatidylinositol 3-kinase activity in epidermal growth factor-stimulated matrix metalloproteinase-9 production and cell surface association. *Cancer Res.* **61,** 1855–1861
45. Lucchesi, P. A., Sabri, A., Belmadani, S., and Matrougui, K. (2004) Involvement of metalloproteinases 2/9 in epidermal growth factor receptor transactivation in pressure-induced myogenic tone in mouse mesenteric resistance arteries. *Circulation* 110, 3587–3593
46. Yoshisue, H., and Hasegawa, K. (2004) Effect of MMP/ADAM inhibitors on goblet cell hyperplasia in cultured human bronchial epithelial cells. *Biosci. Biotechnol. Biochem.* **68,** 2024–2031
47. Fischer, O. M., Hart, S., Gschwind, A., and Ullrich, A. (2003) EGFR signal transactivation in cancer cells. *Biochem. Soc Trans.* **31,** 1203–1208
48. Manning, C. B., Vallyathan, V., and Mossman, B. T. (2002) Diseases caused by asbestos: mechanisms of injury and disease development. *Int. Immunopharmacol.* **2,** 191–200
49. Zanella, C. L., Timblin, C. R., Cummins, A., Jung, M., Goldberg, J., Raabe, R., Tritton, T. R., and Mossman, B. T. (1999) Asbestos-induced phosphorylation of epidermal growth factor receptor is linked to c-fos and apoptosis. *Am. J. Physiol.* **277,** L684–693
50. Manning, C. B., Cummins, A. B., Jung, M. W., Berlanger, I., Timblin, C. R., Palmer, C., Taatjes, D. J., Hemenway, D., Vacek, P., and Mossman, B. T. (2002) A mutant epidermal growth factor receptor targeted to lung epithelium inhibits asbestos-induced proliferation and proto-oncogene expression. *Cancer Res.* **62,** 4169–4175
51. Hornia, A., Lu, Z., Sukezane, T., Zhong, M., Joseph, T., Frankel, P., and Foster, D. A. (1999) Antagonistic effects of protein kinase C alpha and delta on both transformation and phospholipase D activity mediated by the epidermal growth factor receptor. *Mol. Cell. Biol.* **19,** 7672–7680

Received for publication September 2, 2005.
Accepted for publication December 29, 2005.

Cell Stem Cell
Article

Foxo3a Is Essential for Maintenance of the Hematopoietic Stem Cell Pool

Kana Miyamoto,[1,2,9] Kiyomi Y. Araki,[3,9] Kazuhito Naka,[4] Fumio Arai,[1] Keiyo Takubo,[1] Satoshi Yamazaki,[5] Sahoko Matsuoka,[1] Takeshi Miyamoto,[1] Keisuke Ito,[1] Masako Ohmura,[4] Chen Chen,[3] Kentaro Hosokawa,[1] Hiromitsu Nakauchi,[5] Keiko Nakayama,[6] Keiichi I. Nakayama,[7] Mine Harada,[2] Noboru Motoyama,[3,*] Toshio Suda,[1,*] and Atsushi Hirao[4,8,*]

[1]Department of Cell Differentiation, The Sakaguchi Laboratory of Developmental Biology, Keio University School of Medicine, Shinjuku-ku, Tokyo 160-8582, Japan

[2]Department of Medicine and Biosystemic Science, Kyushu University Graduate School of Medical Sciences, Fukuoka, Fukuoka 812-8582, Japan

[3]Department of Geriatric Medicine, National Institute for Longevity Sciences, National Center for Geriatrics and Gerontology, Obu, Aichi 474-8522, Japan

[4]Division of Molecular Genetics, Center for Cancer and Stem Cell Research, Cancer Research Institute, Kanazawa University, Kanazawa, Ishikawa 920-0934, Japan

[5]Laboratory of Stem Cell Therapy, Center for Experimental Medicine, The Institute of Medical Science, University of Tokyo, Minato-ku, Tokyo 108-8639, Japan

[6]Department of Developmental Genetics, Center for Translational and Advanced Animal Research on Human Diseases, Graduate School of Medicine, Tohoku University, Sendai, Miyagi 980-8575, Japan

[7]Department of Molecular and Cellular Biology, Medical Institute of Bioregulation, Kyushu University, Fukuoka, Fukuoka 812-8582, Japan

[8]Core Research for Evolutional Science and Technology, Japan Science and Technology Agency, Kawaguchi, Saitama 332-0012, Japan

[9]These authors contributed equally to this work.

*Correspondence: ahirao@kenroku.kanazawa-u.ac.jp (A.H.), sudato@sc.itc.keio.ac.jp (T.S.), motoyama@nils.go.jp (N.M.)

DOI 10.1016/j.stem.2007.02.01

SUMMARY

Hematopoietic stem cells (HSCs) are maintained in an undifferentiated quiescent state within a bone marrow niche. Here we show that Foxo3a, a forkhead transcription factor that acts downstream of the PTEN/PI3K/Akt pathway, is critical for HSC self-renewal. We generated gene-targeted *Foxo3a*$^{-/-}$ mice and showed that, although the proliferation and differentiation of *Foxo3a*$^{-/-}$ hematopoietic progenitors were normal, the number of colony-forming cells present in long-term cocultures of *Foxo3a*$^{-/-}$ bone marrow cells and stromal cells was reduced. The ability of *Foxo3a*$^{-/-}$ HSCs to support long-term reconstitution of hematopoiesis in a competitive transplantation assay was also impaired. *Foxo3a*$^{-/-}$ HSCs also showed increased phosphorylation of p38MAPK, an elevation of ROS, defective maintenance of quiescence, and heightened sensitivity to cell-cycle-specific myelotoxic injury. Finally, HSC frequencies were significantly decreased in aged *Foxo3a*$^{-/-}$ mice compared to the littermate controls. Our results demonstrate that Foxo3a plays a pivotal role in maintaining the HSC pool.

INTRODUCTION

FOXO transcription factors belong to the forkhead family of transcriptional regulators that is characterized by a conserved DNA binding domain termed the "forkhead box" (Kaestner et al., 2000). The FOXO group of human forkhead proteins contains four members: FOXO1, FOXO3a, FOXO4, and FOXO6. FOXO proteins are normally present in an active state in a cell's nucleus. In response to the binding of growth factors or insulin to the appropriate cell surface receptors, the activation of phosphatidylinositol 3-kinase (PI3K) is triggered. PI3K in turn activates several serine/threonine kinases, including protein kinase B (PKB/Akt) and the related SGK family enzymes (Brunet et al., 1999, 2001; Kops et al., 1999). Activated Akt phosphorylates FOXO proteins at three consensus Akt phosphorylation sites, triggering the inactivation of these molecules and their export from the nucleus into the cytoplasm.

FOXO proteins have both distinct and overlapping functions, and their many target molecules are involved in processes as diverse as cell-cycle arrest (Dijkers et al., 2000a; Furukawa-Hibi et al., 2002; Medema et al., 2000), DNA repair (Furukawa-Hibi et al., 2002; Tran et al., 2002), cellular differentiation (Nakae et al., 2003), and cell death (Brunet et al., 1999; Dijkers et al., 2002; Kaestner et al., 2000). Activation of FOXO proteins occurs in cultured cells subjected to oxidative stress (Brunet et al., 2004; Essers et al., 2004; Furukawa-Hibi et al., 2002; Kobayashi et al., 2005). In *Drosophila* and *C. elegans*, FOXO proteins

Table 1. Blood Cell Counts in 8-Week-Old *Foxo3a*$^{+/+}$ and *Foxo3a*$^{-/-}$ Mice

	Foxo3a$^{+/+}$	*Foxo3a*$^{-/-}$	P Value
WBC (μl)	11,000 ± 4,700	13,000 ± 3,100	NS
RBC (×10^4/μl)	884 ± 79	780 ± 70	<0.01
Hb (g/dl)	13.9 ± 1.0	14.0 ± 1.0	NS
HCT (%)	44.9 ± 2.5	44.7 ± 2.4	NS
MCV (fl)	51.0 ± 2.5	57.5 ± 3.2	<0.01
MCH (pg)	15.8 ± 0.8	18.0 ± 1.0	<0.01
PLT (×10^4/μl)	85.2 ± 12.4	81.0 ± 15.9	NS
Ret (‰)	7.5 ± 0.5	57.5 ± 0.5	<0.01

Values shown are the mean ± SD for 20 mice per genotype. WBC, white blood cell; RBC, red blood cell; Hb, hemoglobin; HCT, hematocrit; MCV, mean corpuscular volume; MCH, mean corpuscular hemoglobin; PLT, platelet; Ret, reticulocyte; NS, not significant.

are involved in regulating metabolism, stress resistance, and longevity (Greer and Brunet, 2005). However, it has yet to be clarified whether FOXO proteins modulate longevity and stress responses in animals. Several mouse models designed to elucidate the physiological functions of the mammalian *Foxo* genes have been reported. *Foxo1*$^{-/-}$ mice die at embryonic day 10.5 (E10.5) due to defective angiogenesis (Furuyama et al., 2004; Hosaka et al., 2004). The principal phenotype of *Foxo3a*$^{-/-}$ mice is an age-dependent female infertility caused by premature activation of the ovarian follicles (Castrillon et al., 2003). *Foxo3a*$^{-/-}$ mice also display hyperproliferation of helper T cells, in line with Foxo3a's known role in promoting cell-cycle arrest (Lin et al., 2004). *Foxo4*$^{-/-}$ mice are viable and do not have an overt phenotype (Hosaka et al., 2004). *Foxo6*$^{-/-}$ mice have yet to be reported.

Mammalian hematopoietic stem cells (HSCs) are maintained in an undifferentiated quiescent state in a bone marrow niche (Arai et al., 2004). It is thought that the mechanisms protecting quiescent HSCs against stress may contribute to the maintenance of the self-renewal capacity and life span of HSCs. We have previously demonstrated that the self-renewal capacity of HSCs depends on Atm-mediated inhibition of oxidative stress (Ito et al., 2004). In the presence of reactive oxygen species (ROS), the p38MAPK pathway is activated such that the HSC population is exhausted. Prolonged treatment of HSCs with an antioxidant or a p38MAPK inhibitor can extend the life span of these cells during serial transplantation, indicating that p38MAPK inactivation protects HSCs against loss of self-renewal capacity (Ito et al., 2006). Thus, it seems that genes or factors related to cellular senescence are involved in regulating the self-renewal capacity of HSCs.

In this study, we demonstrate that Foxo3a is an important contributor to the maintenance of the HSC pool during aging. Our findings have implications for the roles of FOXO proteins in maintenance of tissue homeostasis.

RESULTS

Normal Proliferation, Differentiation, and Apoptosis of Hematopoietic Progenitors in *Foxo3a*$^{-/-}$ Mice

We generated *Foxo3a*$^{-/-}$ mice by disrupting exon 2 of the *Foxo3a* gene with a *neo* cassette (see Figure S1 in the Supplemental Data available at the end of this article). Consistent with a previous report (Castrillon et al., 2003), our *Foxo3a*$^{-/-}$ mice were viable, and female mice showed infertility. To investigate the effect of Foxo3a loss on hematopoiesis, we analyzed the peripheral blood of 8-week-old *Foxo3a*$^{+/+}$ and *Foxo3a*$^{-/-}$ mice. In the latter, we found a decreased number of red blood cells but a significant increase in reticulocytes accompanied by elevations in the mean corpuscular volume (MCV) and mean corpuscular hemoglobin (MCH) (Table 1). These findings indicate that erythropoiesis is abnormal in the absence of Foxo3a, as previously reported (Bakker et al., 2004). However, numbers of white blood cells and platelets were comparable in our *Foxo3a*$^{+/+}$ and *Foxo3a*$^{-/-}$ mice. In addition, lymphoid and myeloid cells in *Foxo3a*$^{-/-}$ peripheral blood and bone marrow (BM) showed wild-type morphology as determined by May Grunwald-Giemsa staining (data not shown). Moreover, flow cytometric analyses of T cell (CD3$^+$), B cell (B220$^+$), and myeloid (Mac-1/Gr-1$^+$) cell populations in *Foxo3a*$^{-/-}$ BM showed that these cells were present at wild-type frequencies (Figure S2). These data indicate that the differentiation of all hematopoietic cells save the erythroid lineage is normal in *Foxo3a*$^{-/-}$ mice.

Next, we investigated the quality and quantity of hematopoietic progenitors in 8- to 12-week-old *Foxo3a*$^{-/-}$ mice. To evaluate the clonogenic capacity and differentiation potential of myeloid and erythroid progenitors, we performed colony-forming assays in vitro in which freshly isolated BM mononuclear cells (MNCs) were cultured for 7 days in methylcellulose medium supplemented with stem cell factor (SCF), thrombopoietin (TPO), erythropoietin (Epo), and granulocyte colony stimulating factor (G-CSF). The numbers and sizes of myeloid (colony-forming unit granulocytes/macrophage, CFU-GM), erythroid (burst-forming unit-erythroid, BFU-E), and mixed (CFU-mix) colonies derived from *Foxo3a*$^{+/+}$ and *Foxo3a*$^{-/-}$ BM MNCs were comparable (Figure 1A). The capacity of *Foxo3a*$^{-/-}$ BM cells to form colonies in the spleen 12 days after transplantation (CFU-S12; short-term repopulating cells) was also equivalent to that of *Foxo3a*$^{+/+}$ BM MNCs (Figure 1B). *Foxo3a*$^{+/+}$ and *Foxo3a*$^{-/-}$ BM also contained similar frequencies of c-Kit$^+$Sca-1$^+$Lineage$^-$ (KSL) cells, which represent a primitive hematopoietic cell fraction containing HSCs and early progenitors (Figure 1C). Furthermore, *Foxo3a*$^{+/+}$ and *Foxo3a*$^{-/-}$ KSL cells demonstrated comparable proliferation and differentiation potential in colony-forming assays (Figure 1D). Because it had been reported that the activation of FOXO by cytokine depletion leads to cell death in hematopoietic cell lines (Dijkers et al., 2000a, 2000b, 2002), we evaluated the apoptosis of

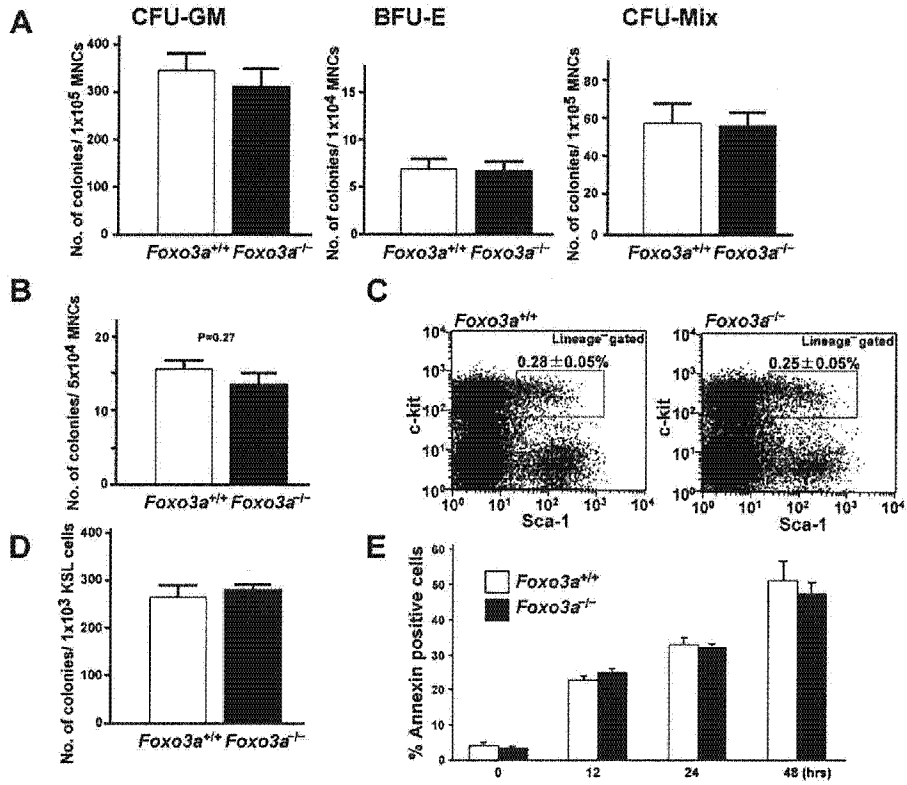

Figure 1. Normal Proliferation, Differentiation, and Apoptosis of Hematopoietic Progenitors in *Foxo3a*$^{-/-}$ Mice

(A) Wild-type in vitro colony formation capacity of *Foxo3a*$^{-/-}$ BM MNCs. BM MNCs from *Foxo3a*$^{+/+}$ and *Foxo3a*$^{-/-}$ mice were cultured with cytokines in methylcellulose medium for 7 days. Data shown are the mean number ± SD of colonies for myeloid (CFU-GM, n = 3), erythroid (BFU-E, n = 3), and mixed (CFU-mix, n = 3) lineages.

(B) Wild-type spleen colony formation by *Foxo3a*$^{-/-}$ BM MNCs. Irradiated mice were transplanted with 5 × 10^4 BM MNCs from *Foxo3a*$^{+/+}$ or *Foxo3a*$^{-/-}$ mice, and spleen colonies were counted on day 12 posttransplant (CFU-S12). Data shown are the mean number ± SD of colonies (n = 5).

(C) Wild-type frequency of KSL cells in the BM of 8-week-old *Foxo3a*$^{-/-}$ mice. c-Kit$^+$Sca-1$^+$ cells in the Lin$^-$ fraction (KSL cells) were detected by flow cytometry. Data shown are a representative pattern of KSL cells. (Insets) Mean percentage ± SD of KSL cells (n = 8).

(D) Wild-type in vitro colony formation capacity of *Foxo3a*$^{-/-}$ KSL cells. KSL cells from *Foxo3a*$^{+/+}$ or *Foxo3a*$^{-/-}$ mice were cultured with cytokines in methylcellulose medium for 7 days. Data shown are the mean number ± SD of colonies (n = 3).

(E) Wild-type apoptosis following cytokine depletion. Lin$^-$ cells from *Foxo3a*$^{+/+}$ and *Foxo3a*$^{-/-}$ mice were cultured without cytokines in serum-supplemented medium for the indicated times and stained with Annexin V. Data shown are the mean percentage ± SD of Annexin V$^+$ cells. No significant differences were observed between *Foxo3a*$^{+/+}$ and *Foxo3a*$^{-/-}$ mice (n = 3).

immature BM cells (Lineage$^-$ cells; Lin$^-$) cultured in the absence of cytokines. However, *Foxo3a*$^{+/+}$ and *Foxo3a*$^{-/-}$ Lin$^-$ cells did not differ in their kinetics of apoptosis (Figure 1E). These results indicate that loss of Foxo3a does not affect the proliferation or differentiation potential of hematopoietic progenitors in the BM of healthy mice.

Abrogated Self-Renewal Capacity of HSCs in the Absence of Foxo3a

To determine if Foxo3a was required for the functions of primitive hematopoietic cells, we carried out long-term cultivation of KSL cells on a layer of OP9 stromal cells. In this assay, the number of colony-forming cells arising after 6 weeks of culture reflects HSC function. The number of colonies derived from *Foxo3a*$^{-/-}$ KSL cells was significantly decreased compared to that derived from *Foxo3a*$^{+/+}$ KSL cells, although short-term cultures (less than 2 weeks) did not show a significant difference (Figure 2A). Thus, the most primitive hematopoietic cells in the BM are profoundly affected by the loss of Foxo3a.

To assess the repopulating capacity of *Foxo3a*$^{-/-}$ HSCs in vivo, we performed a competitive reconstitution assay in which 4 × 10^5 BM MNCs from a *Foxo3a*$^{+/+}$ or *Foxo3a*$^{-/-}$ mouse (CD45.2) competed against an equal number of BM MNCs from a congenic (CD45.1) mouse to reconstitute the hematopoietic compartment of an irradiated recipient mouse (CD45.1). At 16 weeks posttransplantation, flow cytometric analysis of the peripheral blood of the transplanted recipients revealed that *Foxo3a*$^{+/+}$ and *Foxo3a*$^{-/-}$ BM MNCs were equally capable of hematopoietic reconstitution (Figure 2B). We then analyzed the chimerism of donor-derived cells in the BM and found wild-type numbers of *Foxo3a*$^{-/-}$-derived B cells, myeloid cells, and erythroid cells (data not shown) but greatly

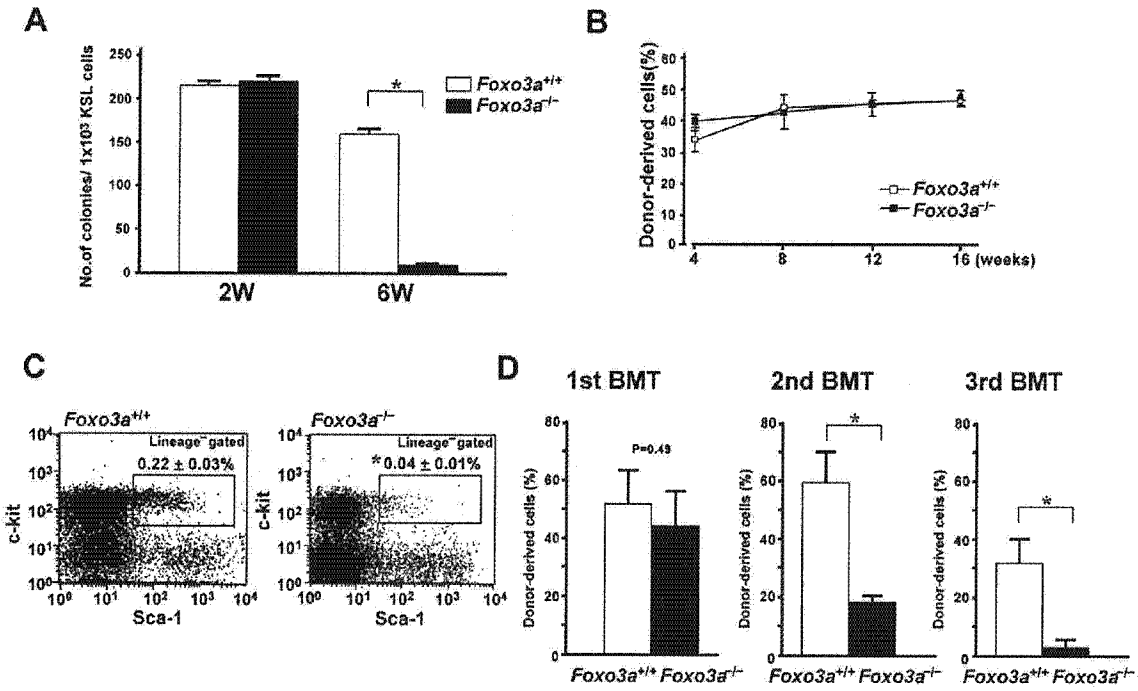

Figure 2. Foxo3a Is Essential for the Self-Renewal of HSCs

(A) Decreased colony formation after long-term culture. *Foxo3a*$^{+/+}$ and *Foxo3a*$^{-/-}$ KSL cells (2 × 10^3) were cultured on OP9 stromal cells for the indicated number of weeks (W) and tested for colony formation. Data shown are the mean number ± SD of colonies formed (*$p < 0.01$, $n = 3$).

(B) Comparable hematopoietic reconstitution capacity of *Foxo3a*$^{+/+}$ and *Foxo3a*$^{-/-}$ BM MNCs. Irradiated recipient mice were transplanted with 4 × 10^5 BM MNCs from *Foxo3a*$^{+/+}$ or *Foxo3a*$^{-/-}$ mice plus 4 × 10^5 competitor cells in a competitive assay as described in the Experimental Procedures. Data shown are the mean percentage ± SD of donor-derived cells in the peripheral blood at the indicated time points after transplantation ($n = 3$).

(C) Defective repopulation of KSL cells derived from *Foxo3a*$^{-/-}$ BM cells after transplantation. BM cells from the recipient mice in (B) were analyzed for the frequency of KSL cells in donor-derived ($CD45.2^+$) MNCs at 16 weeks posttransplantation. Representative data for the frequency of KSL population are shown. (Insets) Mean percentage ± SD of KSL cells in donor-derived MNCs (*$p < 0.01$, $n = 3$).

(D) Defective repopulation capacity of *Foxo3a*$^{-/-}$ BM MNCs during serial transplantation. BM MNCs from the recipient mice were serially transplanted into recipient mice as described in the Experimental Procedures. The repopulating capacity of *Foxo3a*$^{+/+}$ and *Foxo3a*$^{-/-}$ BM donor cells was determined at 16 weeks posttransplant for the first, second, and third BMTs. Data shown are the mean ratio ± SD of donor-derived cells in a competitive assay (*$p < 0.01$, $n = 4$).

reduced numbers of KSL cells (Figure 2C). These results indicate that Foxo3a is not crucial for HSC differentiation but plays a critical role in HSC self-renewal.

To examine the impact of the reduced KSL population derived from *Foxo3a*$^{-/-}$ BM cells on hematopoiesis, we carried out second competitive transplantation. At 16 weeks post first BMT, 1 × 10^6 BM MNCs from these recipients, including donor-derived BM cells (CD45.2), competitor-derived BM cells, and residual recipient BM cells (CD45.1), were transplanted into a second set of recipient mice (CD45.1) (second BMT). At 16 weeks post second BMT, fewer hematopoietic cells in the second recipients were derived from *Foxo3a*$^{-/-}$ BM MNCs compared to *Foxo3a*$^{+/+}$ BM MNCs (Figure 2D), indicating that the reconstituted HSC pool derived from *Foxo3a*$^{-/-}$ BM cells after the first BMT was decreased. At 16 weeks post third BMT, the proportion of *Foxo3a*$^{+/+}$ BM MNC-derived cells was reduced compared to that at 16 weeks post second BMT. This deficit arises presumably because the repopulating capacity of the donor and competitor cells is decreased by repeated BMT, whereas residual recipient BM cells continue to accumulate. Nevertheless, examination of BM cells after a third transplantation revealed a further reduction in the reconstitution capacity of *Foxo3a*$^{-/-}$ BM cells compared to *Foxo3a*$^{+/+}$ BM cells. These data confirm that Foxo3a is essential for the self-renewal capacity of HSCs.

HSC-Specific Dysfunction in *Foxo3a*$^{-/-}$ Mice

We next set out to characterize the cell population most dependent on Foxo3a. As previously reported (Yamazaki et al., 2006), Foxo3a protein is present in the nucleus of freshly isolated *Foxo3a*$^{+/+}$ $CD34^-$KSL cells (HSCs) but appears in the cytoplasm of freshly isolated *Foxo3a*$^{+/+}$ $CD34^+$KSL cells (progenitors) (Figure 3A). When we evaluated the in vitro clonogenic capacity of purified *Foxo3a*$^{+/+}$ $CD34^+$KSL and $CD34^-$KSL cells, we found that $CD34^+$KSL cells generated much larger colonies than did $CD34^-$KSL cells by day 7. However, the clusters (small colonies) derived from $CD34^-$KSL cells caught up

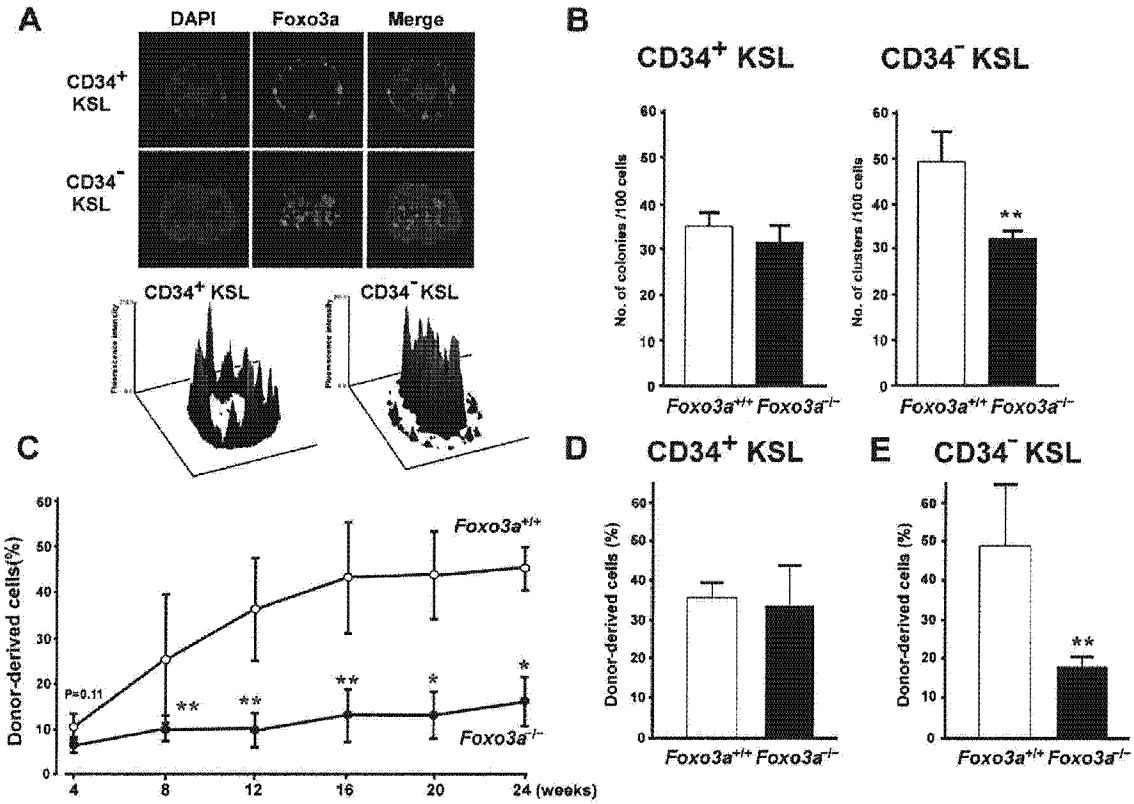

Figure 3. Loss of Foxo3a Results in an HSC-Specific Defect In Vitro and In Vivo

(A) Nuclear localization of Foxo3a in HSCs. (Upper panel) Freshly isolated CD34$^-$ or CD34$^+$KSL cells from *Foxo3a*$^{+/+}$ BM were stained with DAPI (blue) and anti-Foxo3a antibody (red). (Lower panel) The fluorescence intensity of anti-Foxo3a staining at points in each region was plotted as the number of pixels (z axis) relative to the position of these points along the x-y axis.

(B) Defective clonogenic capacity of *Foxo3a*$^{-/-}$ CD34$^-$KSL cells in vitro. CD34$^+$ and CD34$^-$KSL cells from *Foxo3a*$^{+/+}$ or *Foxo3a*$^{-/-}$ mice were cultured in the presence of cytokines in methylcellulose medium for 7 days. Data shown are the mean number of colonies or clusters formed per 100 cells ± SD (**$p < 0.05$, $n = 3$).

(C) Defective long-term reconstitution capacity of *Foxo3a*$^{-/-}$ KSL cells in vivo. Irradiated recipient mice were transplanted with 2×10^5 KSL cells from *Foxo3a*$^{+/+}$ or *Foxo3a*$^{-/-}$ mice plus 4×10^5 competitor cells in a competitive assay. Data shown are the mean percentage ± SD of donor-derived cells in the peripheral blood at indicated time after transplantation (*$P < 0.01$, **$P < 0.05$, $n = 3$).

(D) Comparable short-term hematopoietic reconstitution capacity of *Foxo3a*$^{+/+}$ and *Foxo3a*$^{-/-}$ CD34$^+$KSL cells. Irradiated recipient mice were transplanted with 3.3×10^3 CD34$^+$KSL cells from *Foxo3a*$^{+/+}$ or *Foxo3a*$^{-/-}$ mice plus 4×10^5 competitor cells in a competitive assay. Data shown are the mean percentage ± SD of donor-derived cells in the peripheral blood at 4 weeks after transplantation ($n = 3$).

(E) Defective long-term reconstitution capacity of *Foxo3a*$^{-/-}$ CD34$^-$KSL cells. Recipient mice were transplanted with 200 CD34$^-$KSL cells from *Foxo3a*$^{+/+}$ or *Foxo3a*$^{-/-}$ mice plus 4×10^5 competitor cells in competitive assays, and long-term reconstitution capacity was assessed. Data shown are the mean percentage ± SD of donor-derived cells at 16 weeks posttransplantation (**$p < 0.05$, $n = 4$).

in size by day 14, confirming that CD34$^-$KSL cells are less mature than CD34$^+$KSL cells. When we carried out the same clonogenic assay using *Foxo3a*$^{-/-}$ CD34$^+$KSL and CD34$^-$KSL cells, the numbers of colonies generated by *Foxo3a*$^{+/+}$ and *Foxo3a*$^{-/-}$ CD34$^+$KSL cells were equivalent (Figure 3B). In contrast, the loss of *Foxo3a* resulted in a mild but significant reduction in the number of clusters derived from CD34$^-$KSL cells. Despite this decrease in number, the differentiation potential of the clusters derived from CD34$^-$KSL cells was not obviously affected by Foxo3a deficiency (Figure S3). These data indicate that loss of Foxo3a results in a defect in in vitro clonogenic capacity that is specific to HSCs.

To evaluate HSC function in vivo, we evaluated the repopulating capacity of purified KSL cells using the competitive reconstitution assay. At 4 weeks posttransplantation, the repopulating capacity of *Foxo3a*$^{-/-}$ KSL cells was comparable to that of *Foxo3a*$^{+/+}$ KSL cells, suggesting that loss of Foxo3a does not affect progenitor function (Figure 3C). However, at later time points in the experiment, the repopulating capacity of *Foxo3a*$^{-/-}$ KSL cells was lower than that of *Foxo3a*$^{+/+}$ KSL cells. These data suggested that Foxo3a deficiency might cause an in vivo defect that impaired the function of HSCs but not that of progenitors. To confirm the effect of Foxo3a deficiency on HSC function in vivo, we examined the

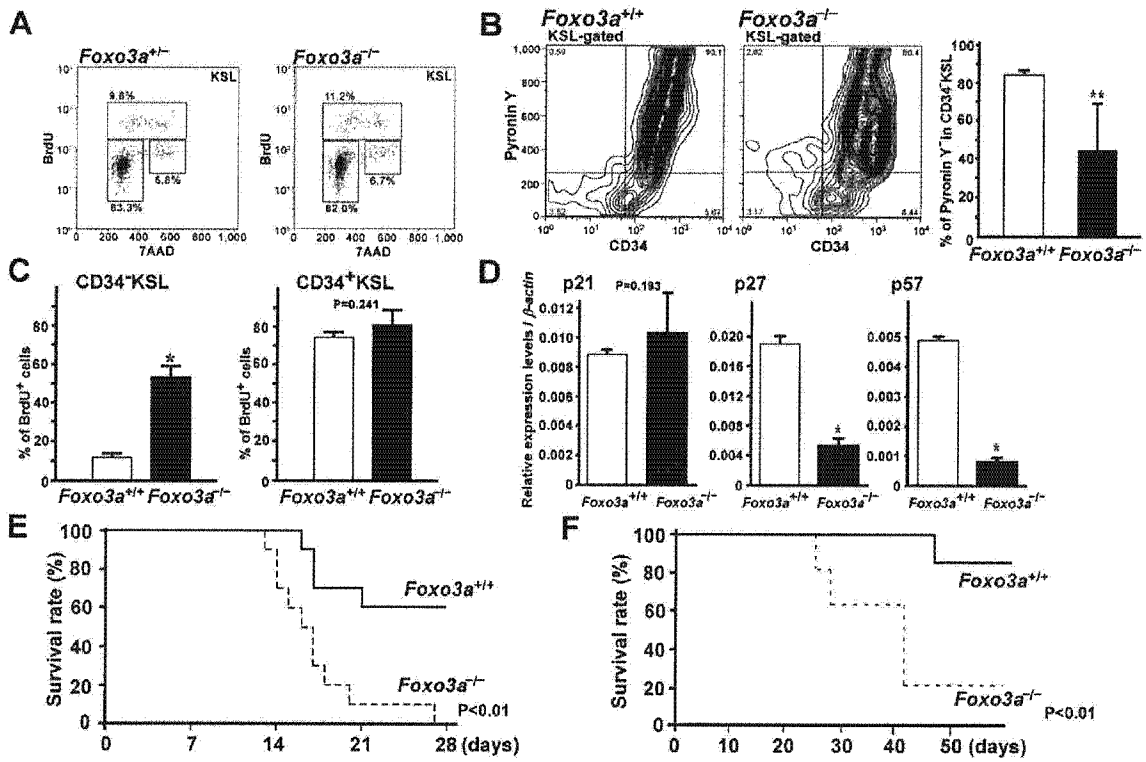

Figure 4. Defect in the Maintenance of HSC Quiescence in *Foxo3a*$^{-/-}$ Mice

(A) Equivalent cell-cycle status of *Foxo3a*$^{+/-}$ and *Foxo3a*$^{-/-}$ KSL cells. Two hours after i.p. injection of BrdU into *Foxo3a*$^{+/-}$ or *Foxo3a*$^{-/-}$ mice, KSL cells were isolated and stained with anti-BrdU antibody and 7AAD to evaluate cell-cycle status. (Insets) Percentages of cells in G1, S, or G2/M phase. Results shown are one cell-cycle analysis representative of three independent experiments.

(B) Reduced frequency of quiescent cells in the CD34$^-$KSL population. CD34$^-$KSL cells of *Foxo3a*$^{+/+}$ or *Foxo3a*$^{-/-}$ mice were stained with Pyronin Y and analyzed by flow cytometry. (Left and middle panels) Results of one trial representative of four independent experiments. (Right panel) The mean percentage ± SD of Pyronin Y$^-$ cells in the CD34$^-$KSL population (**$p < 0.05$, $n = 4$).

(C) Increased BrdU incorporation in *Foxo3a*$^{-/-}$ CD34$^-$KSL cells. BrdU was administered orally to *Foxo3a*$^{+/+}$ and *Foxo3a*$^{-/-}$ mice for 7 days, and BrdU incorporation in CD34$^+$ or CD34$^-$KSL cells was evaluated by using anti-BrdU antibody. Data shown are the mean percentage ± SD of BrdU$^+$ cells in the CD34$^-$KSL (left panel) or CD34$^+$KSL (right panel) populations (*$p < 0.01$, $n = 3$).

(D) Decreased p27 and p57 expression in *Foxo3a*$^{-/-}$ CD34$^-$KSL cells. The relative mRNA expression levels of p21, p27, and p57 in CD34$^-$KSL cells from *Foxo3a*$^{+/+}$ or *Foxo3a*$^{-/-}$ mice were evaluated by quantitative real-time RT-PCR and normalized to β-actin expression. Data shown are the mean ratio ± SD of transcript levels over β-actin (*$p < 0.01$, $n = 3$).

(E and F) Increased sensitivity to myelotoxic stress. (E) *Foxo3a*$^{+/+}$ and *Foxo3a*$^{-/-}$ mice ($n = 10$) were i.p. injected with 5-FU (150 mg/kg) weekly, and survival was monitored daily. Data shown are the survival rates expressed as a percentage. Results were analyzed with a log-rank nonparametric test. (F) Irradiated recipient mice ($n = 6$) transplanted with *Foxo3a*$^{+/+}$ or *Foxo3a*$^{-/-}$ BM cells were subjected to the same 5-FU protocol. Survival rate was determined as for (E).

short-term reconstitution capacity of CD34$^+$KSL progenitors, as well as the long-term reconstitution capacity of CD34$^-$KSL HSCs, in competitive transplantation assays. *Foxo3a*$^{-/-}$ CD34$^+$KSL cells supported normal reconstitution of hematopoiesis in short-term (4 weeks) experiments (Figure 3D), consistent with our earlier finding that Foxo3a is not involved in CD34$^+$KSL function. In contrast, the loss of Foxo3a in CD34$^-$KSL HSCs led to a significant defect in reconstitution by 16 weeks posttransplantation (Figure 3E), indicating that Foxo3a is essential for the long-term repopulating capacity of HSCs. Since anemia was not observed in recipient mice (data not shown), the defect in the erythroid lineage did not affect the repopulating capacity of *Foxo3a*$^{-/-}$ HSCs. Thus, *Foxo3a*$^{-/-}$ mice have a profound defect in HSC function, but not in progenitor function.

Failure of Quiescence Maintenance in *Foxo3a*$^{-/-}$ HSCs

HSCs are normally maintained in an undifferentiated quiescent state (G0 phase), and this quiescence protects HSCs against losing self-renewal capacity. To evaluate the quiescence status of HSCs in *Foxo3a*$^{-/-}$ mice, we first examined the cell-cycle status of KSL cells using BrdU (5-bromodeoxyuridine) incorporation. No differences were found between *Foxo3a*$^{+/-}$ and *Foxo3a*$^{-/-}$ mice in the percentage of KSL cells that had undergone cell division over a 2 hr period (Figure 4A). Obvious apoptosis was not observed in either *Foxo3a*$^{+/+}$ or *Foxo3a*$^{-/-}$ KSL cells (Fig-

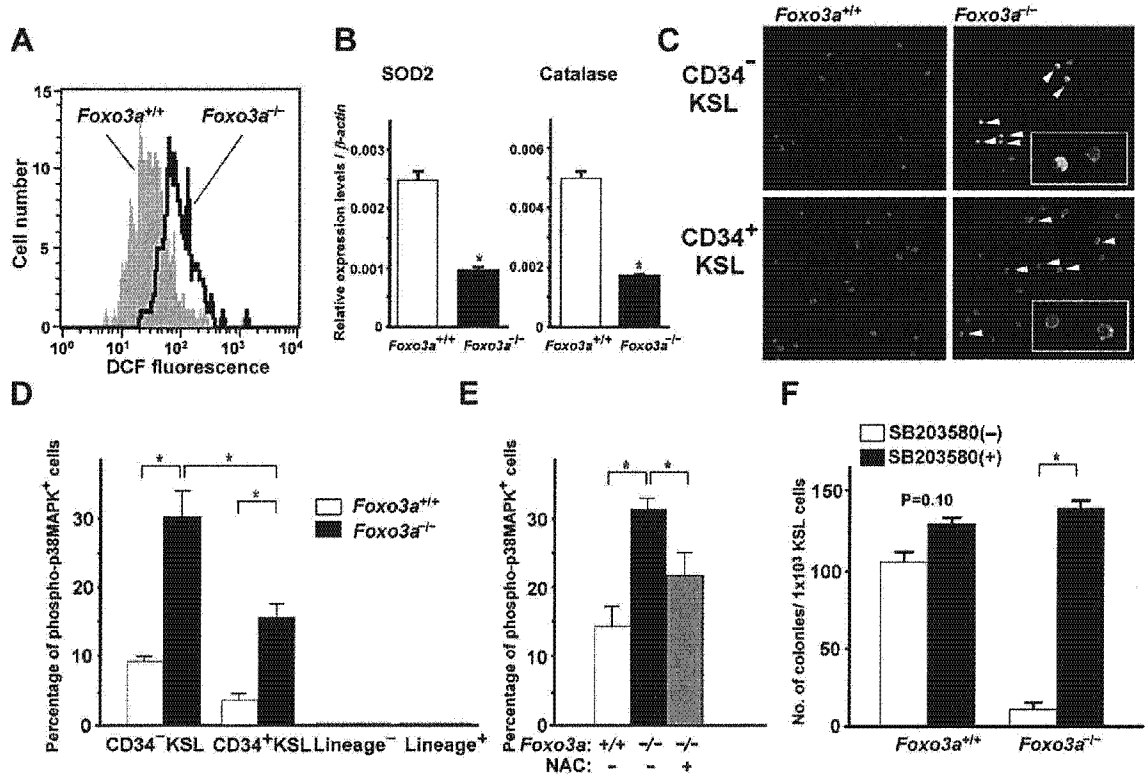

Figure 5. Impaired HSC Function by p38MAPK Activation in *Foxo3a*$^{-/-}$ Mice

(A) Elevation of ROS. Intracellular H_2O_2 concentrations of *Foxo3a*$^{+/+}$ and *Foxo3a*$^{-/-}$ KSL cells were determined by the DCFDA assay. Data shown are representative of three independent experiments.

(B) Reduced SOD2 and catalase expressions. The mRNA expression levels of SOD2 and catalase were determined in *Foxo3a*$^{+/+}$ and *Foxo3a*$^{-/-}$ CD34$^-$KSL cells using quantitative real time RT-PCR and normalized to β-actin expression. Data shown are the mean ratio ± SD of transcript levels over β-actin (*$p < 0.01$, $n = 3$).

(C and D) Increased p38MAPK phosphorylation. CD34$^-$ and CD34$^+$KSL cells from *Foxo3a*$^{+/+}$ and *Foxo3a*$^{-/-}$ mice were stained with anti-phospho-p38MAPK mAb. DAPI staining (blue) was used to detect nuclei. Representative data are shown in (C). Arrowheads, phospho-p38MAPK$^+$ cells. (Insets) Higher magnification of representative phospho-p38MAPK$^+$ cells. Data shown in (D) are the mean percentage ± SD of phospho-p38MAPK$^+$ cells in the CD34$^-$, CD34$^+$, Lin$^-$, and Lin$^+$ fractions of BM cells from *Foxo3a*$^{+/+}$ and *Foxo3a*$^{-/-}$ mice (*$p < 0.01$, $n = 5$).

(E) Inhibition of p38MAPK phosphorylation by NAC treatment. *Foxo3a*$^{+/+}$ and *Foxo3a*$^{-/-}$ mice were administered NAC in vivo and p38MAPK activation in *Foxo3a*$^{+/+}$ and *Foxo3a*$^{-/-}$ CD34$^-$KSL cells was determined as for (D). Data shown are the mean percentage ± SD of phospho-p38 MAPK$^+$ cells in the CD34$^-$KSL cell population (*$p < 0.01$, $n = 3$).

(F) Restored colony-forming capacity after long-term culture with a p38MAPK inhibitor. *Foxo3a*$^{+/+}$ and *Foxo3a*$^{-/-}$ mice KSL cells were cultured on OP9 stromal cells with or without 10 μM SB203580 for 6 weeks, and colony formation assays were performed as for Figure 2A. Data shown are the mean number ± SD of colonies formed (*$p < 0.01$, $n = 3$).

ure S4). To directly evaluate HSC quiescence in *Foxo3a*$^{-/-}$ mice, we stained CD34$^-$KSL cells from *Foxo3a*$^{+/+}$ and *Foxo3a*$^{-/-}$ mice with Pyronin Y, an agent that specifically and quantitatively stains double-stranded RNA and accurately reflects the G0 phase (Huttmann et al., 2001). Consistent with previous work (Yamazaki et al., 2006), we found that most *Foxo3a*$^{+/+}$ CD34$^-$KSL cells stained negatively for Pyronin Y, indicating normal HSC quiescence. However, a sizable Pyronin Y$^+$ population was detected among *Foxo3a*$^{-/-}$ CD34$^-$KSL cells (Figure 4B). To investigate whether *Foxo3a*$^{-/-}$ CD34$^-$KSL cells were cycling in vivo, BrdU was administered to mice orally for 7 days. Whereas *Foxo3a*$^{+/+}$ CD34$^-$KSL cells showed minimal BrdU incorporation, almost 60% of *Foxo3a*$^{-/-}$ cells were BrdU$^+$ (Figure 4C). These results indicate that Foxo3a deficiency drives HSCs to abandon the G0 phase and enter the cell cycle. With respect to the CD34$^+$KSL population, 70%–80% of these cells were BrdU$^+$ in both *Foxo3a*$^{+/+}$ and *Foxo3a*$^{-/-}$ mice. The defect in HSC quiescence in the absence of Foxo3a was further supported by the finding of decreased levels of the negative cell-cycle regulators p27 and p57 in *Foxo3a*$^{-/-}$ CD34$^-$KSL cells (Figure 4D).

Cheng et al. have reported that loss of p21 leads to a failure in the maintenance of HSC quiescence. In this case, when the mutant animals were exposed to the cell-cycle-specific myelotoxic drug 5-FU as an exogenous stress, they died prematurely due to hematopoietic

cell depletion (Cheng et al., 2000). These observations prompted us to investigate the sensitivity of *Foxo3a*$^{-/-}$ mice and their hematopoietic cells to weekly 5-FU treatments. Although some 5-FU-treated *Foxo3a*$^{+/+}$ mice died at 2 weeks after the initial injection, fully 60% of them survived until at least 4 weeks postinjection (Figure 4E). In contrast, all *Foxo3a*$^{-/-}$ mice were dead within 4 weeks after the first injection, showing that Foxo3a is required for normal HSC resistance to 5-FU. To exclude the possibility that the death of the mice was due to the toxic effects of 5-FU on other tissues, we repopulated the hematopoietic system of lethally irradiated recipients with either *Foxo3a*$^{+/+}$ or *Foxo3a*$^{-/-}$ BM cells. Four months after transplantation, we challenged the reconstituted mice with weekly 5-FU treatments. A similar increase in mortality was observed in mice transplanted with *Foxo3a*$^{-/-}$ BM cells as compared to those bearing *Foxo3a*$^{+/+}$ BM cells (Figure 4F). Thus, 5-FU-treated *Foxo3a*$^{-/-}$ mice die prematurely due to effects on the hematopoietic system and not because of the sensitivity of other tissues to the antimetabolite treatment. Foxo3a therefore protects hematopoietic cells from destruction by cell-cycle-dependent myelotoxic agents, and a loss of Foxo3a leads to hematopoietic cell depletion and premature death of the animal. Taken together, our data demonstrate that Foxo3a plays a pivotal role in the maintenance of HSC quiescence and suggest that Foxo3a functions to protect HSCs against exogenous stress.

Impaired HSC Function by p38MAPK Activation in *Foxo3a*$^{-/-}$ Mice

We have previously reported that p38MAPK activation induced by ROS elevation promotes exhaustion of HSCs during serial BM transplantation (Ito et al., 2006). We therefore evaluated ROS levels and the activation status of p38MAPK in HSCs of *Foxo3a*$^{+/+}$ and *Foxo3a*$^{-/-}$ mice. ROS was indeed increased in *Foxo3a*$^{-/-}$ KSL cells compared to *Foxo3a*$^{+/+}$ KSL cells (Figure 5A). Moreover, the expression levels of SOD2 and catalase, two Foxo target genes involved in ROS detoxification (Essers et al., 2004; Kops et al., 2002; Nemoto and Finkel, 2002), were significantly downregulated in *Foxo3a*$^{-/-}$ CD34$^-$KSL cells (Figure 5B). When p38MAPK phosphorylation was examined in hematopoietic cell subsets of *Foxo3a*$^{+/+}$ and *Foxo3a*$^{-/-}$ mice, fewer than 10% of CD34$^-$KSL cells in *Foxo3a*$^{+/+}$ mice showed p38MAPK phosphorylation (Figures 5C and 5D). In contrast, p38MAPK was phosphorylated in approximately 30% of *Foxo3a*$^{-/-}$ CD34$^-$KSL cells. Interestingly, we found that more CD34$^-$KSL cells than CD34$^+$KSL cells showed p38MAPK phosphorylation in *Foxo3a*$^{-/-}$ BM but that neither Lin$^-$ nor Lin$^+$ cells had significant levels of phosphorylated p38MAPK. This increased phosphorylation of p38MAPK in *Foxo3a*$^{-/-}$ CD34$^-$KSL cells could be significantly inhibited by prior administration to the mice of the antioxidant N-acetyl-L-cysteine (NAC), although it was a partial effect (Figure 5E). Finally, we evaluated the effect of a p38MAPK inhibitor (SB203580) on the ability of *Foxo3a*$^{-/-}$ cells to generate colonies after 6 weeks of culture (a reflection of HSC function). We found that the colony-forming capacity of *Foxo3a*$^{-/-}$ KSL cells subjected to long-term culture could be restored by treatment with 10 μM SB203580 (Figure 5F). In the absence of this p38MAPK inhibitor, the number of colonies generated from *Foxo3a*$^{-/-}$ cells was reduced to the levels previously shown in Figure 2A, indicating that p38MAPK activation impairs HSC function.

Decreased HSC Pool in Aged *Foxo3a*$^{-/-}$ Mice

All the data presented above were obtained from studies of young adult (8- to 12-week-old) *Foxo3a*$^{+/+}$ and *Foxo3a*$^{-/-}$ mice. Despite the defective HSC self-renewal capacity in *Foxo3a*$^{-/-}$ mice, the frequency of CD34$^-$KSL cells in these mutants was similar to that in *Foxo3a*$^{+/+}$ mice (Figure S5). Thus, a loss of Foxo3a does not influence HSC numbers in vivo in young adult mice. However, it was quite possible that the defect in self-renewal capacity could lead to a shortened HSC life span in vivo that would become evident as the mice aged. We therefore evaluated hematopoiesis in aged *Foxo3a*$^{+/+}$ and *Foxo3a*$^{-/-}$ mice and observed that the peripheral blood of aged *Foxo3a*$^{-/-}$ mice did not show any signs of progressive hematopoietic failure (Table S1). However, there was a reduction in the frequency of CD34$^-$KSL cells in aged *Foxo3a*$^{-/-}$ mice as compared to the littermate controls (Figures 6A and 6B and Figure S6). As previously reported (Rossi et al., 2005; Sudo et al., 2000), the frequency of CD34$^-$KSL population in aged *Foxo3a*$^{+/+}$ mice was higher than that in young mice. Our aged *Foxo3a*$^{-/-}$ mice did not show the expansion of CD34$^-$KSL cells seen in aged wild-type mice. The frequency of the CD34$^+$KSL progenitor population was reduced in some, but not all, aged *Foxo3a*$^{-/-}$ mice. These results indicate that the loss of *Foxo3a* had its dominant effect on the HSC population in aged animals. To investigate the effect of aging on HSC function, we evaluated repopulating capacity of aged *Foxo3a*$^{-/-}$ HSCs. When we carried out the clonogenic assay using KSL cells from aged *Foxo3a*$^{-/-}$ mice, we found reduced colony formation activity in aged *Foxo3a*$^{-/-}$ mice (Figure 6C), in contrast to the results obtained for young *Foxo3a*$^{-/-}$ mice (Figure 1D). Similarly, when we carried out long-term cultivation of KSL cells from aged *Foxo3a*$^{-/-}$ mice on a layer of OP9 stromal cells, the number of colony-forming cells arising after 2 weeks of culture was dramatically decreased (Figure 6D) in a manner not observed for KSL cells from young *Foxo3a*$^{-/-}$ mice (Figure 2A). Furthermore, the long-term repopulating capacity of BM MNCs from aged *Foxo3a*$^{-/-}$ mice was significantly reduced compared to that of BM MNCs from aged *Foxo3a*$^{+/+}$ mice (Figure 6E), in contrast to the results obtained for young *Foxo3a*$^{+/+}$ and *Foxo3a*$^{-/-}$ mice (Figure 2B). These data demonstrate that the defect in repopulation capacity of aged *Foxo3a*$^{-/-}$ HSCs was more severe than that of young *Foxo3a*$^{-/-}$ HSCs. We therefore conclude that the loss of Foxo3a leads to a defect in the self-renewal capacity of HSCs that impairs the maintenance of in vivo HSC pool during aging.

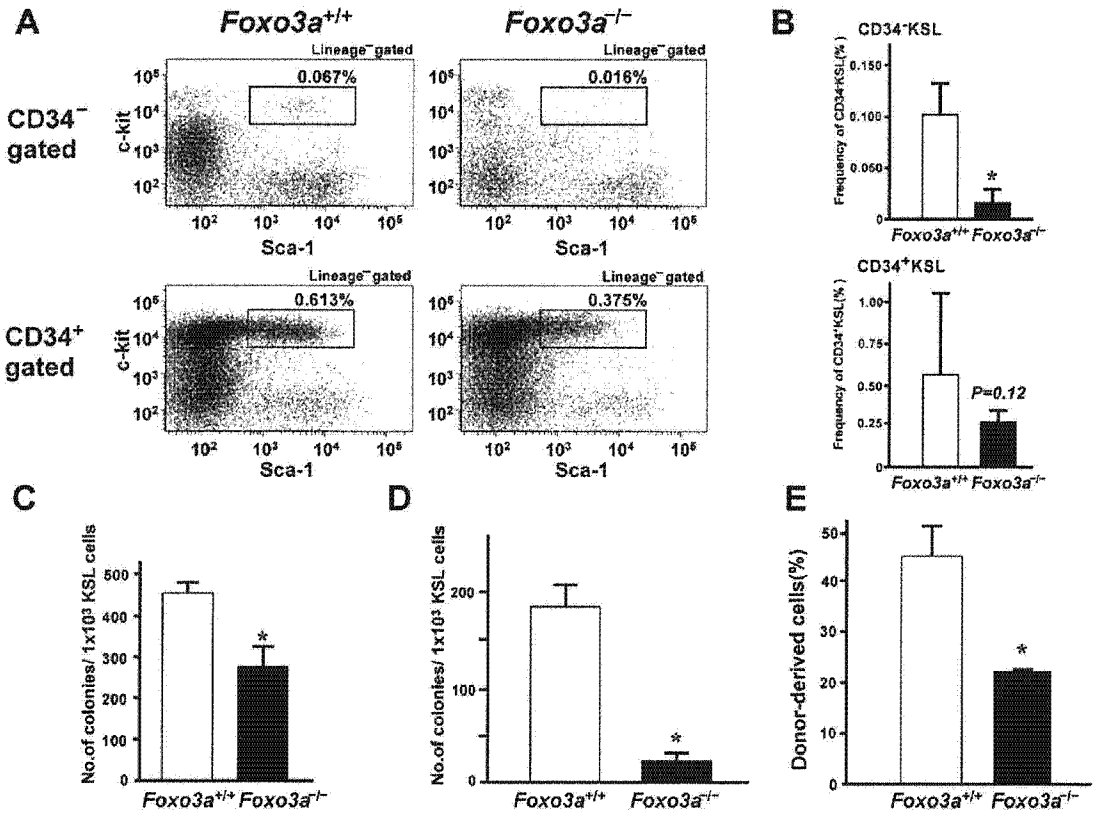

Figure 6. Decreased HSC Pool in Aged *Foxo3a*$^{-/-}$ Mice

(A) CD34$^-$KSL (upper panels) and CD34$^+$KSL (lower panels) cells from 80-week-old *Foxo3a*$^{+/+}$ or *Foxo3a*$^{-/-}$ mice were analyzed by flow cytometry. (Insets) Percentage of CD34$^-$ or CD34$^+$KSL cells in total BM MNCs.

(B) Mean frequency ± SD of CD34$^-$KSL (upper panel) and CD34$^+$KSL (lower panel) cells in aged *Foxo3a*$^{-/-}$ mice compared to littermate *Foxo3a*$^{+/+}$ mice (56–108 weeks old) (*$p < 0.01$, $n = 6$).

(C) Reduced in vitro colony formation capacity. KSL cells from aged *Foxo3a*$^{+/+}$ or *Foxo3a*$^{-/-}$ mice were cultured with cytokines in methylcellulose medium for 7 days. Data shown are the mean number ± SD of colonies formed ($n = 3$).

(D) Decreased colony formation after long-term culture. KSL cells (2×10^3) from aged *Foxo3a*$^{+/+}$ and *Foxo3a*$^{-/-}$ mice were cultured on OP9 stromal cells for 2 weeks and tested for colony formation. Data shown are the mean number ± SD of colonies formed (*$p < 0.01$, $n = 3$).

(E) Defective long-term reconstitution capacity of BM MNCs from aged *Foxo3a*$^{-/-}$ mice. Irradiated recipient mice were transplanted with 1×10^6 *Foxo3a*$^{+/+}$ or *Foxo3a*$^{-/-}$ BM MNCs plus 1×10^6 competitor cells in a competitive assay. Data shown are the mean percentage ± SD of donor-derived cells in the peripheral blood at 12 weeks after transplantation (*$p < 0.01$, $n = 3$).

DISCUSSION

The self-renewal of postnatal HSCs is closely coupled to their slow cell cycling or quiescence, and the maintenance of HSC quiescence is thought to be a requisite for sustaining a self-renewing HSC compartment. Here we show that *Foxo3a*$^{-/-}$ HSCs can neither maintain quiescence nor support long-term reconstitution of hematopoiesis. The mutant HSCs exhibit increased phosphorylation of p38MAPK, show a heightened sensitivity to cell-cycle-specific myelotoxic injury, and lose self-renewal capacity during aging.

In quiescent wild-type HSCs, Akt is not activated, and Foxo proteins are localized in the nucleus (Yamazaki et al., 2006). Upon cytokine stimulation of these HSCs in vitro, Akt becomes activated and induces the export of Foxo proteins from the nucleus to the cytoplasm. In conjunction with this export, the HSCs lose their repopulating capacity. Attenuation of cytokine signaling by lipid raft inhibitors maintains both HSC quiescence and nuclear localization of Foxo proteins (Yamazaki et al., 2006). These findings suggest that the fine tuning of cytokine signals within a niche can influence Foxo localization, which in turn governs HSC quiescence. It has been reported that FOXO regulates the expression of p21 and p27 (Dijkers et al., 2000a; Medema et al., 2000; Seoane et al., 2004). In this study, we observed decreased expression of p27 and p57, but not p21, in *Foxo3a*$^{-/-}$ HSCs. We therefore speculate that, in our mutant mice, the loss of Foxo3a may have directly reduced the expression of multiple negative regulators of the cell cycle, resulting in the observed defect in the maintenance of

HSC quiescence. On the other hand, *Foxo3a*$^{-/-}$ HSCs showed elevated ROS as well as reduced expression of SOD2 and catalase, two Foxo targets that are involved in ROS detoxification (Essers et al., 2004; Kops et al., 2002; Nemoto and Finkel, 2002). Because ROS elevation disrupts the maintenance of HSC quiescence, it may be that Foxo3a deficiency causes HSC cell cycle abnormalities via ROS dysregulation. We previously reported that p38MAPK activation induced by oxidative stress leads to a defect in HSC self-renewal capacity (Ito et al., 2006). Consistent with this finding, our present study showed that Foxo3a contributes to maintain HSC capacity mediated by repression of p38MAPK activation. However, ROS-independent pathway might induce p38MAPK activation in *Foxo3a*$^{-/-}$ HSCs, because NAC treatment partially restored p38MAPK status.

Our knowledge of the physiological intrinsic cues regulating HSC maintenance and expansion remains limited. The tumor suppressor Pten (phosphatase and tensin homolog) has been found to regulate HSC maintenance through restriction of HSC proliferation (Yilmaz et al., 2006; Zhang et al., 2006). The finding is especially interesting to us, as PTEN acts upstream of FOXO. Pten deficiency leads to activation of PI3K that results in Akt activation and consequently Foxo inactivation. This relationship could theoretically underlie the similarities in the phenotypes of Pten-deficient and *Foxo3a*$^{-/-}$ HSCs with respect to cell cycle regulation and repopulating capacity, although our *Foxo3a*$^{-/-}$ mice do not develop leukemia. Yilmaz et al. reported that the mTOR inhibitor rapamycin not only depleted leukemia-initiating cells in Pten-deficient mice but also restored normal HSC function, indicating that mTOR activation causes the loss of HSC function in these animals (Yilmaz et al., 2006). Since it has recently been reported that rapamycin can indirectly inhibit Akt activation (Sarbassov et al., 2006), the possibility thus exists that rapamycin treatment restores HSC function by promoting Foxo activation. It will be interesting to determine whether Foxo3a acts downstream of Pten to regulate HSC function.

Despite the fundamental importance of HSCs and Foxo3a's role in their maintenance, our *Foxo3a*$^{-/-}$ mice did not show any obvious abnormalities in embryogenesis, aging, or function of the hematopoietic system in the absence of exogenous stress. The extreme subtlety of the phenotypes of *Foxo3a*$^{-/-}$ mice is likely due to compensation by other Foxo family members. While this manuscript was under review, phenotypes by conditional deletions of Foxo1, -3a, and -4 genes were reported (Paik et al., 2007; Tothova et al., 2007). Tothova et al. demonstrated that deletions of triple genes lead to marked decrease of KSL population with increased apoptosis and cell cycling caused by an elevation of ROS. Deficiency of Foxo3a single gene did not show any phenotypes in KSL population, consistent with our data. Since phenotypes of aged *Foxo3a*$^{-/-}$ mice were more severe than those of young mice in our study, the compensatory effects by other family members may be attenuated during aging.

Stem cells and progenitors are now known to exist in a variety of tissues. Tissue-specific stem cells continuously give rise to mature cells throughout the life of an animal and maintain the homeostasis of a particular tissue. Our study shows that Foxo3a is essential for the maintenance of the self-renewal capacity of HSCs in vivo. It has been reported that Foxo family members regulate the differentiation potential of progenitors (Bakker et al., 2004; Hribal et al., 2003). Since the aging of an organism may be driven in part by a gradual depletion of the functional capacity of tissue-specific stem cells, Foxo3a might be involved in controlling physiological aging mediated by regulating stem cell capacity in a variety of tissues. Furthermore, manipulation of Foxo3a may represent a novel approach to regenerative medicine. It may be possible in the future to establish a culture system in which Foxo3a activation is modified such that HSCs can expand while maintaining their repopulating capacity. If such a modification of FOXO function can be generalized to stem cells of other tissues, this approach could be useful for enhancing or sustaining tissue regenerative capacity in vivo.

EXPERIMENTAL PROCEDURES

Mice and Blood Cell Counts

Foxo3a$^{-/-}$ mice were generated as described in the Supplemental Experimental Procedures and in Figure S1. Heterozygous *Foxo3a*$^{+/-}$ mice were subsequently intercrossed to generate *Foxo3a*$^{-/-}$ mice in C57BL/6 (F4). Littermates were used as controls in all experiments. C57BL/6 CD45.1 congenic mice (B6-CD45.1) were purchased from Sankyo-Lab Service (Tsukuba, Japan). Animal care in our laboratory was in accordance with the guidelines for animal and recombinant DNA experiments of the National Institute for Longevity Sciences, Keio University and Kanazawa University. NAC was administrated orally (40 mM in drinking water) for 4 weeks. For analysis of blood counts, peripheral blood from the postorbital vein was collected in a heparinized microtube (Drummond Scientific) and analyzed on a CellTac (NIHON KOHDEN).

Flow Cytometry

Monoclonal antibodies (mAbs) recognizing the following markers were used for flow cytometric analyses and cell sorting (FACS Vantage or FACS Aria, BD Bioscience): c-Kit (2B8), Sca-1 (E13-161.7), CD4 (L3T4), CD8 (53-6.7), B220 (RA3-6B2), TER-119 (Ly-76), Gr-1 (RB6-8C5), CD34 (RAM34), CD71 (R17217), CD45.1(A20), CD45.2(104), and anti-Mac-1 (M1/70). All mAbs were purchased from BD Biosciences. A mixture of mAbs recognizing CD4, CD8, B220, TER-119, Mac-1, or Gr-1 was used to identify Lin$^+$ cells.

Colony-Forming Assays

For long-term cultures, 2 × 10^3 KSL cells were cocultured with OP9 stromal cells as previously described (Ito et al., 2004) After 2–6 weeks' culture, cells were harvested and used for hematopoietic colony-forming assays. For some experiments, the p38MAPK inhibitor SB203580 (Calbiochem) was added at 10 μM to long-term cultures. Methylcellulose colony-forming assays were performed with 20 ng/ml SCF (Pepro Tech EC Ltd.), 20 ng/ml interleukin-3 (PeproTech EC Ltd.), 2 U/ml Epo (Chugai Pharmaceutical Co., Ltd.), and 20 ng/ml G-CSF (Kirin Brewery Co., Ltd.) as previously described (Arai et al., 2004). For the day 12 CFU spleen (CFU-S12) assay, 5 × 10^4 BM MNCs were injected

into lethally irradiated mice. Colonies growing in the spleen were fixed and counted 12 days after injection as previously described (Ito et al., 2004).

Competitive Reconstitution Assay

Lethally irradiated C57BL/6-CD45.1 congenic mice were reconstituted with BM MNCs, KSL cells, $CD34^+KSL$ cells, or $CD34^-KSL$ cells from *Foxo3a*$^{+/+}$ or *Foxo3a*$^{-/-}$ mice (CD45.2), in competition with BM MNCs from C57BL/6-CD45.1 mice. Reconstitution of donor-derived cells (CD45.2) was monitored by staining blood cells with mAbs against CD45.2, CD45.1, CD3, B220, Mac-1, and Gr-1. For the serial transplantation analysis, BM cells (1×10^6) were obtained from recipient mice at 16 weeks posttransplantation (first BMT) and transplanted into a second set of lethally irradiated mice (second BMT). Subsequent transplantations were performed in the same manner.

5-FU Treatment

5-FU (Kyowa Hakko) was administered to mice intraperitoneally (i.p.) at a dose of 150 mg/kg once per week for 3 weeks, and the survival of individual mice was monitored daily.

Intracellular ROS Assay

The cells were incubated with 300 nM CM-H_2-DCFDA (Invitrogen) at 37°C for 5 min followed by analysis of fluorescence by flow cytometry.

Cell-Cycle Analyses

Analysis of the G0 phase by Pyronin Y staining was performed as previously described (Yamazaki et al., 2006). To determine KSL cell-cycle status by BrdU incorporation in vivo, BrdU (100 mg/kg; Sigma) was injected i.p. into *Foxo3a*$^{+/-}$or *Foxo3a*$^{-/-}$ mice. At 2 hr postinjection, KSL cells were collected from BM, fixed, and stained with 7AAD and anti-BrdU antibody (BD Biosciences) as previously described (van Pelt et al., 2005). For analysis of in vivo BrdU incorporation in $CD34^-KSL$ cells, BrdU was administered to mice orally for 7 days (1 mg/ml in sterile deionized water), and $CD34^-KSL$ cells were collected by flow cytometry. The isolated $CD34^-KSL$ cells were fixed and treated with anti-BrdU antibody as above.

Apoptosis

Lin^- cells were collected from total BM cells using the MACS cell separator system (Miltenyi Biotec). Lin^- cells were stained with propidium iodide (PI) and Annexin V (R & D Systems) to detect apoptotic cells.

Immunocytochemistry

Immunocytochemistry of $CD34^-$ and $CD34^+KSL$ cells was performed as previously described (Yamazaki et al., 2006). Briefly, cells were directly sorted onto a glass slide, fixed with 4% paraformaldehyde (PFA), and stained with anti-Foxo3a mAb (Upstate Cell Signaling Solutions) or anti-phospho-p38MAPK mAb (Cell Signaling Technology). Nuclei were identified by staining with DAPI or TOTO-3 (Invitrogen). Subcellular localizations were determined by using confocal microscopy. The fluorescence intensity of each region was analyzed by National Institutes of Health Image.

RT-PCR

cDNAs were reverse-transcribed from total RNA prepared from $CD34^-KSL$ cells. To quantify transcripts, cDNA was subjected to real-time PCR using SYBR Premix Ex Taq (Takara Bio) in Real-Time PCR System Mx3000P (Stratagene). Amplification of β-actin was used for sample normalization. Primer sequences are as follow: p21, 5′-CCGCTGGAGGGCAACTTCGT-3′, 5′-TTTCGGCCCTGAGATGTTCC-3′; p27/Kip1, 5′-TCTCAGGCAAACTCTGAGGAC-3′, 5′-TTCGGAGCTGTTTACGTCTGG-3′; p57/Kip2, 5′-TGATGAGCTGGGAACTGAGCC-3′, 5′-ACGTCGTTCGACGCCTTGTTC-3′; SOD2, 5′-CCCAGACCTGCCTTACGACTAT-3′, 5′-TCTCCCAGTTGATTACATTCCA-3′; Catalse, 5′-GGGAACCCAATAGGAGATAAACTT-3′, 5′-GGTCACTGAACAAGAAAGAAACCT-3′; and β-actin, 5′-AGGTCATCACTATTGGCAACGA-3′, 5′-CACTTCATGATGGAATTGAATGTAGTT-3′.

Statistical Analyses

P values were calculated by using the unpaired Student's t test except for the 5-FU experiments. Survival rates following 5-FU treatment were analyzed with a log-rank nonparametric test.

Supplemental Data

Supplemental Data include Supplemental Experimental Procedures, six figures, and one table and can be found at the end of this document.

ACKNOWLEDGMENTS

We thank Dr. Atsushi Iwama for helpful discussion and Ayami Ono and Yukari Yamada for technical assistance. A.H. was supported by the Grant-in-Aid for Stem Cell Research from the Ministry of Education, Culture, Sports, Science, and Technology, Japan. T.S. was supported by the Grant-in-Aid for Specially Promoted Research from the Ministry of Education, Culture, Sports, Science, and Technology, Japan. N.M. was supported by the Grant-in-Aid for Comprehensive Research on Aging and Health from the Ministry of Health, Labour, and Welfare, Japan. The authors declare that they have no competing financial interests.

Received: November 22, 2006
Revised: January 22, 2007
Accepted: February 21, 2007
Published online: March 15, 2007

REFERENCES

Arai, F., Hirao, A., Ohmura, M., Sato, H., Matsuoka, S., Takubo, K., Ito, K., Koh, G.Y., and Suda, T. (2004). Tie2/angiopoietin-1 signaling regulates hematopoietic stem cell quiescence in the bone marrow niche. Cell *118*, 149–161.

Bakker, W.J., Blazquez-Domingo, M., Kolbus, A., Besooyen, J., Steinlein, P., Beug, H., Coffer, P.J., Lowenberg, B., von Lindern, M., and van Dijk, T.B. (2004). FoxO3a regulates erythroid differentiation and induces BTG1, an activator of protein arginine methyl transferase 1. J. Cell Biol. *164*, 175–184.

Brunet, A., Bonni, A., Zigmond, M.J., Lin, M.Z., Juo, P., Hu, L.S., Anderson, M.J., Arden, K.C., Blenis, J., and Greenberg, M.E. (1999). Akt promotes cell survival by phosphorylating and inhibiting a Forkhead transcription factor. Cell *96*, 857–868.

Brunet, A., Park, J., Tran, H., Hu, L.S., Hemmings, B.A., and Greenberg, M.E. (2001). Protein kinase SGK mediates survival signals by phosphorylating the forkhead transcription factor FKHRL1 (FOXO3a). Mol. Cell. Biol. *21*, 952–965.

Brunet, A., Sweeney, L.B., Sturgill, J.F., Chua, K.F., Greer, P.L., Lin, Y., Tran, H., Ross, S.E., Mostoslavsky, R., Cohen, H.Y., et al. (2004). Stress-dependent regulation of FOXO transcription factors by the SIRT1 deacetylase. Science *303*, 2011–2015.

Castrillon, D.H., Miao, L., Kollipara, R., Horner, J.W., and DePinho, R.A. (2003). Suppression of ovarian follicle activation in mice by the transcription factor Foxo3a. Science *301*, 215–218.

Cheng, T., Rodrigues, N., Shen, H., Yang, Y., Dombkowski, D., Sykes, M., and Scadden, D.T. (2000). Hematopoietic stem cell quiescence maintained by p21cip1/waf1. Science *287*, 1804–1808.

Dijkers, P.F., Medema, R.H., Lammers, J.W., Koenderman, L., and Coffer, P.J. (2000a). Expression of the pro-apoptotic Bcl-2 family member Bim is regulated by the forkhead transcription factor FKHR-L1. Curr. Biol. *10*, 1201–1204.

Dijkers, P.F., Medema, R.H., Pals, C., Banerji, L., Thomas, N.S., Lam, E.W., Burgering, B.M., Raaijmakers, J.A., Lammers, J.W., Koenderman, L., et al. (2000b). Forkhead transcription factor FKHR-L1 modulates cytokine-dependent transcriptional regulation of p27(KIP1). Mol. Cell. Biol. *20*, 9138–9148.

Dijkers, P.F., Birkenkamp, K.U., Lam, E.W., Thomas, N.S., Lammers,

J.W., Koenderman, L., and Coffer, P.J. (2002). FKHR-L1 can act as a critical effector of cell death induced by cytokine withdrawal: protein kinase B-enhanced cell survival through maintenance of mitochondrial integrity. J. Cell Biol. *156*, 531–542.

Essers, M.A., Weijzen, S., de Vries-Smits, A.M., Saarloos, I., de Ruiter, N.D., Bos, J.L., and Burgering, B.M. (2004). FOXO transcription factor activation by oxidative stress mediated by the small GTPase Ral and JNK. EMBO J. *23*, 4802–4812.

Furuyama, T., Kitayama, K., Shimoda, Y., Ogawa, M., Sone, K., Yoshida-Araki, K., Hisatsune, H., Nishikawa, S., Nakayama, K., Nakayama, K., et al. (2004). Abnormal angiogenesis in Foxo1 (Fkhr)-deficient mice. J. Biol. Chem. *279*, 34741–34749.

Furukawa-Hibi, Y., Yoshida-Araki, K., Ohta, T., Ikeda, K., and Motoyama, N. (2002). FOXO forkhead transcription factors induce G(2)-M checkpoint in response to oxidative stress. J. Biol. Chem. *277*, 26729–26732.

Greer, E.L., and Brunet, A. (2005). FOXO transcription factors at the interface between longevity and tumor suppression. Oncogene *24*, 7410–7425.

Hosaka, T., Biggs, W.H., III, Tieu, D., Boyer, A.D., Varki, N.M., Cavenee, W.K., and Arden, K.C. (2004). Disruption of forkhead transcription factor (FOXO) family members in mice reveals their functional diversification. Proc. Natl. Acad. Sci. USA *101*, 2975–2980.

Hribal, M.L., Nakae, J., Kitamura, T., Shutter, J.R., and Accili, D. (2003). Regulation of insulin-like growth factor-dependent myoblast differentiation by Foxo forkhead transcription factors. J. Cell Biol. *162*, 535–541.

Huttmann, A., Liu, S.L., Boyd, A.W., and Li, C.L. (2001). Functional heterogeneity within rhodamine123(lo) Hoechst33342(lo/sp) primitive hemopoietic stem cells revealed by Pyronin Y. Exp. Hematol. *29*, 1109–1116.

Ito, K., Hirao, A., Arai, F., Matsuoka, S., Takubo, K., Hamaguchi, I., Nomiyama, K., Hosokawa, K., Sakurada, K., Nakagata, N., et al. (2004). Regulation of oxidative stress by ATM is required for self-renewal of haematopoietic stem cells. Nature *431*, 997–1002.

Ito, K., Hirao, A., Arai, F., Takubo, K., Matsuoka, S., Miyamoto, K., Ohmura, M., Naka, K., Hosokawa, K., Ikeda, Y., et al. (2006). Reactive oxygen species act through p38 MAPK to limit the lifespan of hematopoietic stem cells. Nat. Med. *12*, 446–451.

Kaestner, K.H., Knochel, W., and Martinez, D.E. (2000). Unified nomenclature for the winged helix/forkhead transcription factors. Genes Dev. *14*, 142–146.

Kobayashi, Y., Furukawa-Hibi, Y., Chen, C., Horio, Y., Isobe, K., Ikeda, K., and Motoyama, N. (2005). SIRT1 is critical regulator of FOXO-mediated transcription in response to oxidative stress. Int. J. Mol. Med. *16*, 237–243.

Kops, G.J., de Ruiter, N.D., De Vries-Smits, A.M., Powell, D.R., Bos, J.L., and Burgering, B.M. (1999). Direct control of the Forkhead transcription factor AFX by protein kinase B. Nature *398*, 630–634.

Kops, G.J., Dansen, T.B., Polderman, P.E., Saarloos, I., Wirtz, K.W., Coffer, P.J., Huang, T.T., Bos, J.L., Medema, R.H., and Burgering, B.M. (2002). Forkhead transcription factor FOXO3a protects quiescent cells from oxidative stress. Nature *419*, 316–321.

Lin, L., Hron, J.D., and Peng, S.L. (2004). Regulation of NF-kappaB, Th activation, and autoinflammation by the forkhead transcription factor Foxo3a. Immunity *21*, 203–213.

Medema, R.H., Kops, G.J., Bos, J.L., and Burgering, B.M. (2000). AFX-like Forkhead transcription factors mediate cell-cycle regulation by Ras and PKB through p27kip1. Nature *404*, 782–787.

Nakae, J., Kitamura, T., Kitamura, Y., Biggs, W.H., III, Arden, K.C., and Accili, D. (2003). The forkhead transcription factor Foxo1 regulates adipocyte differentiation. Dev. Cell *4*, 119–129.

Nemoto, S., and Finkel, T. (2002). Redox regulation of forkhead proteins through a p66shc-dependent signaling pathway. Science *295*, 2450–2452.

Paik, J.H., Kollipara, R., Chu, G., Ji, H., Xiao, Y., Ding, Z., Miao, L., Tothova, Z., Horner, J.W., Carrasco, D.R., et al. (2007). FoxOs are lineage-restricted redundant tumor suppressors and regulate endothelial cell homeostasis. Cell *128*, 309–323.

Rossi, D.J., Bryder, D., Zahn, J.M., Ahlenius, H., Sonu, R., Wagers, A.J., and Weissman, I.L. (2005). Cell intrinsic alterations underlie hematopoietic stem cell aging. Proc. Natl. Acad. Sci. USA *102*, 9194–9199.

Sarbassov, D.D., Ali, S.M., Sengupta, S., Sheen, J.H., Hsu, P.P., Bagley, A.F., Markhard, A.L., and Sabatini, D.M. (2006). Prolonged rapamycin treatment inhibits mTORC2 assembly and Akt/PKB. Mol. Cell *22*, 159–168.

Seoane, J., Le, H.V., Shen, L., Anderson, S.A., and Massague, J. (2004). Integration of Smad and forkhead pathways in the control of neuroepithelial and glioblastoma cell proliferation. Cell *117*, 211–223.

Sudo, K., Ema, H., Morita, Y., and Nakauchi, H. (2000). Age-associated characteristics of murine hematopoietic stem cells. J. Exp. Med. *192*, 1273–1280.

Tothova, Z., Kollipara, R., Huntly, B.J., Lee, B.H., Castrillon, D.H., Cullen, D.E., McDowell, E.P., Lazo-Kallanian, S., Williams, I.R., Sears, C., et al. (2007). FoxOs are critical mediators of hematopoietic stem cell resistance to physiologic oxidative stress. Cell *128*, 325–339.

Tran, H., Brunet, A., Grenier, J.M., Datta, S.R., Fornace, A.J., Jr., DiStefano, P.S., Chiang, L.W., and Greenberg, M.E. (2002). DNA repair pathway stimulated by the forkhead transcription factor FOXO3a through the Gadd45 protein. Science *296*, 530–534.

van Pelt, K., de Haan, G., Vellenga, E., and Daenen, S.M. (2005). Administration of low-dose cytarabine results in immediate S-phase arrest and subsequent activation of cell cycling in murine stem cells. Exp. Hematol. *33*, 226–231.

Yamazaki, S., Iwama, A., Takayanagi, S., Morita, Y., Eto, K., Ema, H., and Nakauchi, H. (2006). Cytokine signals modulated via lipid rafts mimic niche signals and induce hibernation in hematopoietic stem cells. EMBO J. *25*, 3515–3523.

Yilmaz, O.H., Valdez, R., Theisen, B.K., Guo, W., Ferguson, D.O., Wu, H., and Morrison, S.J. (2006). Pten dependence distinguishes haematopoietic stem cells from leukaemia-initiating cells. Nature *441*, 475–482.

Zhang, J., Grindley, J.C., Yin, T., Jayasinghe, S., He, X.C., Ross, J.T., Haug, J.S., Rupp, D., Porter-Westpfahl, K.S., Wiedemann, L.M., et al. (2006). PTEN maintains haematopoietic stem cells and acts in lineage choice and leukaemia prevention. Nature *441*, 518–522.

[Full Paper]

Efficient electroblotting of gel-resolved proteins onto diamond-like carbon-coated plate for protein-chip

Yoko Ino[1], Akiko Okayama[1], Yuko Iwafune[1], Noriaki Arakawa[1], Julia Kikuchi[1], Masahiro Kamita[1], Hiroshi Kawasaki[1], Takeshi Okada[2] and Hisashi Hirano[1]

SUMMARY

We have developed a technique, which can produce high-density protein chips. In this technique, proteins are separated by gel electrophoresis, and electroblotted by semidry blotting apparatus onto a diamond-like carbon-coated stainless-steel plate (DLC plate) of which surface is modified chemically with amino groups. Proteins immobilized on this protein chip can interact with other proteins in solution, and proteins interacted with the immobilized proteins can be identified by mass spectrometric analysis. However, the electroblotting efficiency was not stable. We anticipated that the unstable efficiency might be related to the fluctuation of temperature during electroblotting. In the present study, to investigate the optimal temperature for efficient and effective electroblotting, we developed a semidry blotting apparatus, which could regulate blotting temperature from 4 to 45°C (±1°C). The high and reproducible blotting efficiency was obtained at not low temperature but rather high temperature (30°C). The temperature did not impede protein identification or analysis of protein-protein interactions on the DLC plates by mass spectrometry.

Key words: gel electrophoresis, electroblotting, protein chip, DLC plate, protein interaction.

INTRODUCTION

For proteome analysis, protein chips are a promising tool to profile expressed proteins, such as disease-associated proteins, and to analyze protein-protein, protein-DNA, and protein-drug interactions[1–4]. Recently, we developed a novel protein chip plate, on which proteins separated by gel electrophoresis can be electroblotted[5]. This plate was made of stainless-steel, which was coated with diamond-like carbon and its surface was chemically modified with either N-hydroxysuccinimide ester or amino groups, which can bind proteins covalently or non-covalently proteins, respectively. Using this diamond-like carbon-coated stainless-steel plate (DLC plate) as a protein chip plate, we established a technique with mass spectrometry such as matrix-assisted laser desorption ionization/time-of-flight mass spectrometry (MALDI-TOF MS) to identify the proteins immobilized on the DLC plate after separation of gel electrophoresis. We also developed a novel technique with MALDI-TOF MS to detect proteins that interact with the proteins transferred to the plates from the gels after gel electrophoresis.

However, the electroblotting efficiency from the gels to the DLC plate was sometimes low. We anticipated that the low efficiency might be related to the fluctuation of temperature during electroblotting. Therefore, we constructed a semidry electroblotting apparatus that controls the electroblotting temperature precisely, and investigated the optimal temperature condition for electroblotting in the present study. We found that electroblotting was stable and reproducible at relatively high temperature (30°C), and this temperature did not impede protein identification or protein-protein interaction analysis by MS.

[1] International Graduate School of Arts and Sciences, Yokohama City University, Japan.
[2] SUS Co., Japan.
Correspondence address: Hisashi Hirano; International Graduate School of Arts and Sciences, Yokohama City University, Maioka 641-12, Totsuka, Yokohama, Kanagawa 244-0813, Japan.
Abbreviations: DLC plate, diamond-like carbon coated stainless steel plate; MALDI-TOF MS, matrix assisted laser desorption ionization/ time-of-flight mass spectrometry.
(Received September 29, 2006, Accepted October 31, 2006, Published December 15, 2006)

MATERIALS AND METHODS

Proteins

Fluorescent labeling reagent, CyDye, phosphorylase b, bovine serum albumin, ovalbumin, and carbonic anhydrase were purchased from GE Healthcare (Milwaukee, WI, USA). Soybean lectin and concanavalin A were obtained from Wako (Osaka, Japan).

Detection of proteins labeled with CyDye

The Cy3-labeled proteins that became immobilized on the DLC plate were detected by Typhoon 9410 (GE Healthcare) at an excitation wavelength of 532 nm and emission filter of 580 nm. The detected fluorescence was analyzed by ImageQuant (GE Healthcare).

Production of the DLC plate

The diamond-like carbon film was deposited on a stainless-steel plate by the ion-assisted deposition method[6]. Briefly, the plate was put into a reactor evacuated under 8×10^{-3} Pa using a turbo molecular pump, and then plasma-cleaned by applying hydrogen as a feed gas. The hydrogen gas flow rate was controlled at 40 sccm, and the self-bias radio frequency power for the plate was 100 W. After the treatment, methane and hydrogen gases were introduced into the reactor at flow rates of 47.5 sccm and 2.5 sccm, respectively, to deposit the diamond-like carbon film onto the plate at ambient temperature. The working pressure in the reactor and the radio frequency power for the plate were maintained at 3 Pa and 200 W, respectively. The surface of the diamond-like carbon film was aminated by plasma, using ammonium as the feed gas at an 18-sccm flow rate and 3-Pa working pressure. Finally, the plate was rinsed with deionized water and dried under a vacuum at 100°C.

Production of temperature-controlled semidry blotting apparatus

We constructed a semidry blotting apparatus, consisting of a carbon plate cathode, a stainless-steel plate anode, and a constant-temperature regulator.

SDS-gel electrophoresis

We performed SDS-PAGE using the method of Laemmli[7], with modifications. We used thin slab gels (80×60×0.3 mm), and performed the electrophoresis at 5 mA.

Electroblotting of gel-resolved proteins onto the DLC plates

After electrophoresis, the gel was soaked in 10% (v/v) methanol for 30 sec, and then freshly prepared 10% methanol for 3 min. The proteins were then electroblotted onto the DLC plate from the gel in the semidry blotting apparatus. We used 0.5 M borate buffer (pH 8.0) as a blotting solution. Two pieces of filter paper (3MM; Whatman, Florham Park, NJ, USA) were soaked in the blotting solution, and excess solution on the gel or filter paper was removed. The DLC plate, the gel, a piece of wetted cellophane, and the two pieces of saturated filter paper were stacked, in that order, from the anode of the semidry blotting apparatus and sandwiched between the carbon cathode and stainless-steel anode electrode plates.

Mass spectrometric analysis of the blotted proteins

Cy3-labeled proteins were separated by gel electrophoresis, immobilized on the DLC plate. After immobilization, 1 μl of protease solution containing 15 μg/ml trypsin (Promega, Madison, WI, USA) in 5 mM NH_4HCO_3 (pH 8.0) was dispensed onto the DLC plate. The DLC plate was placed in a Petri dish and proteins were digested overnight at 37°C in a humidified environment. After digestion, the matrix solution, which was saturated with alpha-cyano-4-hydroxycinnamic acid in 40% (v/v) acetonitrile/0.1% (v/v) trifluoroacetic acid, was delivered to the top of the target zone of each protein position on the DLC plate. The digests were analyzed using an Axima MALDI-TOF MS (Shimadzu, Kyoto, Japan). The proteins immobilized on the DLC plate were identified by peptide mass fingerprinting, using the Mascot Server (http://www.matrixscience.com/).

RESULTS

Production of temperature-controlled semidry blotting apparatus

The semidry blotting apparatus, in which temperatures from 4 to 45°C (±1°C) could be controlled accurately, was manufactured to examine the effect of temperature on the transfer of gel-resolved proteins onto the DLC plates (Fig. 1). The apparatus consisted of a carbon cathode electrode plate (Fig. 1b), a stainless-steel anode plate (Fig. 1c), and a thermoregulator (Fig. 1d).

Protein electroblotting

Two proteins, phosphorylase b and bovine serum albumin, were separated by SDS-PAGE on 0.3-mm-thick gels, and the separated proteins were electroblotted from the gels onto the DLC plate in the temperature-controlled semidry blotting apparatus. The electroblotting was performed with a 500 μA constant current for 1 h at five different temperatures (10, 15, 20, 30, and 35°C) to investigate whether temperature affects blotting efficiency. The blotting efficiency at 10 and 15°C was uniformly low for both phosphorylase b and bovine serum albumin. Efficiency increased as the temperature rose. The highest efficiency was obtained at 30°C (Fig. 2). The efficiency at 35°C was not measured because the gel became partially dried during blotting, making the transfer of proteins impossible.

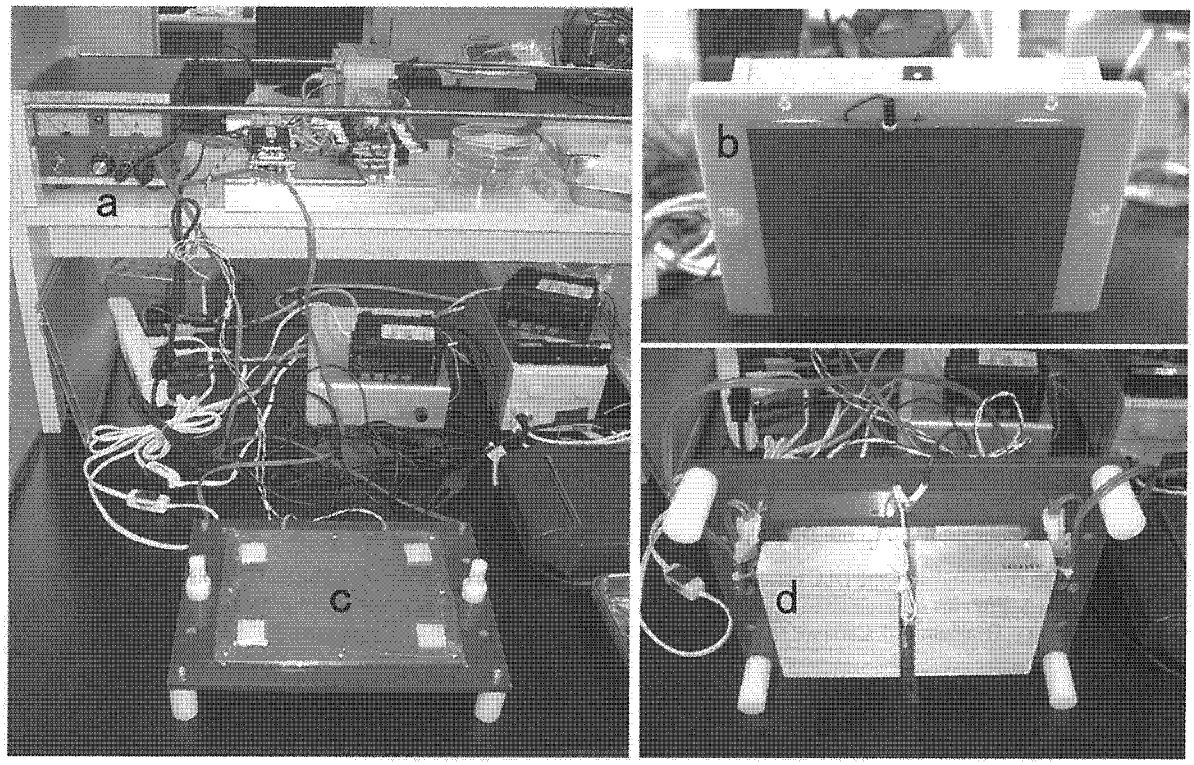

Fig. 1. Temperature-controlled semidry blotting apparatus.

a, Power supply; b, Carbon cathode plate; c, Stainless-steel anode plate; d, Thermoregulator under the anode plate (c).

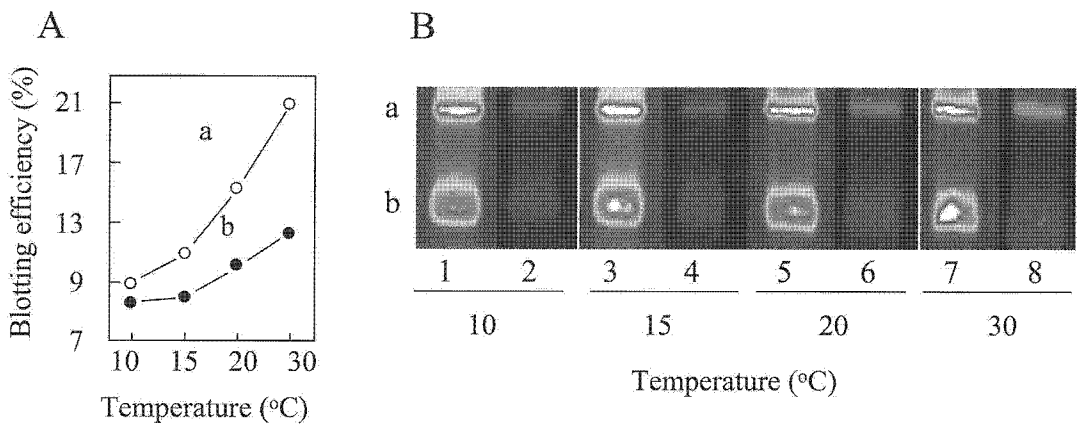

Fig. 2. A, Blotting efficiency of phosphorylase b and bovine serum albumin at different electroblotting temperatures (10, 15, 20, and 30°C). B, Detection of Cy3-labeled proteins. a, Phosphorylase b; b, Bovine serum albumin; lanes 1, 3, 5, and 7, Gels after electroblotting; lanes 2, 4, 6, and 8, DLC plate after electroblotting; lanes 1 and 2, 10°C; lanes 3 and 4, 15°C; lanes 5 and 6, 20°C; lanes 7 and 8, 30°C.

Mass spectrometry of blotted proteins

Phosphorylase b, bovine serum albumin, ovalbumin, and carbonic anhydrase were separated by SDS-PAGE and electroblotted onto the DLC plates at 30°C (Fig. 3A). Trypsin was added to the blotted proteins, which were digested overnight. After digestion, the matrix solution was added for mass-spectrometric analysis, and the DLC plate was analyzed using MALDI-TOF MS. All four proteins were successfully identified by MS analysis after peptide mass fingerprinting (Fig. 3B).

In addition, soybean lectin was separated by SDS-PAGE and transferred onto the DLC plate, after which concanavalin A was reacted with the immobilized lectin (Fig. 4A). The lectin and concanavalin A were digested with trypsin on the DLC plate and analyzed by MALDI-TOF MS. As Fig. 4B shows, the MS analysis yielded the spectra of both proteins, which were identified by a database search.

DISCUSSION

Protein chips

The DLC plate protein chips are suitable for high-throughput analysis of protein expression and protein-

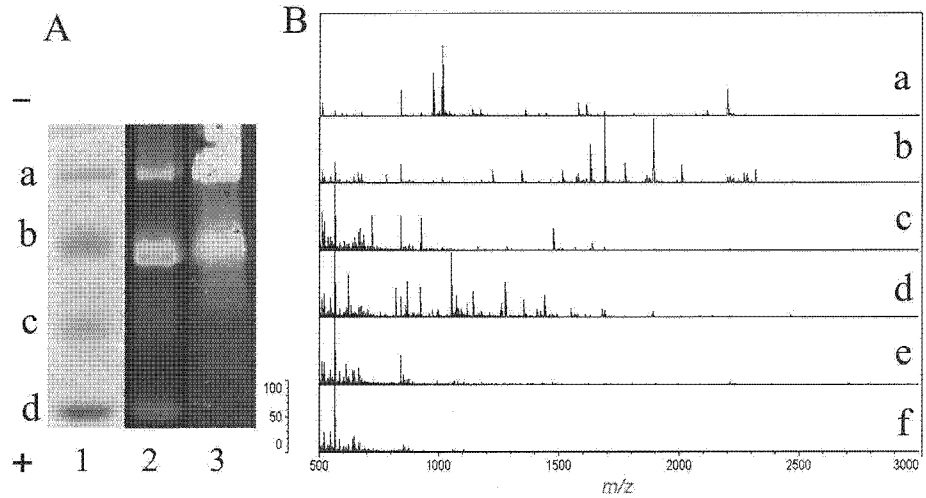

Fig. 3. Mass spectra of four proteins on the DLC plate.

A, Proteins electroblotted onto the DLC plate from the gel at 30°C. Lane 1, Proteins separated by SDS-PAGE; lane 2, Proteins remaining in the gel; lane 3, Proteins electroblotted onto the DLC plate; B, Peptide mass fingerprints of four proteins. a, Phosphorylase b; b, Bovine serum albumin; c, Ovalbumin; d, Carbonic anhydrase, e, Trypsin; f, Matrix.

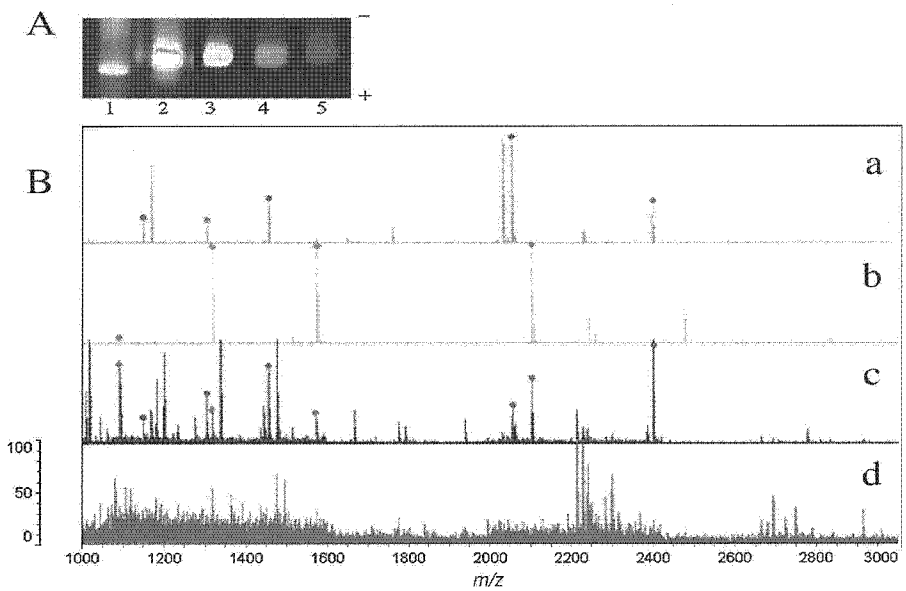

Fig. 4. A, The interaction of Cy3-labeled lectin with Cy5-labeled concanavalin A (Con A) transferred from the gel to the DLC plate at 30°C. Lanes 1 and 2, Mr marker proteins and Cy3-labeled lectin, respectively, separated by SDS-PAGE; lane 3, Cy3-labeled lectin transferred to the DLC plate; lane 4, Cy3-labeled lectin interacted with Con A on the DLC plate; lane 5, Cy5-labeled Con A interacted with lectin on the DLC plate. lanes 1–4, Cy3 detection; lane 5, Cy5 detection. B, Mass spectra of Con A and lectin interacted on the DLC plate. Cy3-labeled lectin was separated by SDS-PAGE and electroblotted onto the DLC plate. After blocking, the DLC plate was incubated with buffer solution containing Cy5-labeled Con A. The proteins on the DLC plate were digested with trypsin. The digests were measured by MALDI-TOF MS to identify the proteins using peptide mass fingerprinting. a, Lectin; b, Con A; c, Con A/lectin complex; d, Trypsin.

protein and protein-ligand interactions. Iwafune et al.[5] developed the protein chip technology, using a number of proteins separated by gel electrophoresis and electroblotted onto a DLC plate. In that study, proteins that became immobilized on the DLC plate were digested with proteases, such as trypsin, lysylendopeptidase, and Asp-specific protease, for identification by peptide mass fingerprinting analysis using MALDI-TOF MS. The mass spectra showed that the proteins on the protein chip could be identified. The study also showed that proteins on the DLC plate could interact with proteins in the extract and that these proteins could also be identified by on-plate digestion, followed by MALDI-TOF MS analysis.

However, the protein blotting efficiency was inconsistent, even for the same protein, suggesting that the data were not easily reproducible. One factor implicated in the inconsistent results was the temperature fluctuation during electroblotting. We constructed a semidry blotting appara-

tus to strictly control the temperature during electroblotting and examined the relationship between blotting efficiency and blotting temperature.

Electroblotting apparatus

Our semidry blotting apparatus can control blotting temperatures ranging from 4 to 45°C (±1°C). Until now, these apparatuses could only regulate low temperatures, and ours is the first to enable the investigation of high-temperature effects on electroblotting.

Separation of proteins by gel electrophoresis

Generally, 1-mm-thick gels are used when proteins are separated by SDS-PAGE. However, we used 0.3-mm-thick gels, as the electroblotting was performed at a very low current (or voltage) to prevent the electrolysis of the DLC plate surfaces[5]. Blotting efficiency decreased sharply when 1-mm-thick gels were used. We found that the efficiency of 0.3-mm-thick gels was 30–70% higher than that of 1-mm-thick gels.

Electroblotting temperature

The heat generated during electroblotting may be a factor in protein denaturing, gel dehydration, and DLC plate defoliation. Therefore, electroblotting is usually performed at a low temperature. During the initial stage of this study, when we also used low temperatures for electroblotting, the blotting efficiency was not stable. We demonstrated that high and reproducible protein electroblotting efficiency occurs, not at low temperatures, but at a relatively high temperature (30°C).

Identification of proteins by MS

To examine whether proteins could be electroblotted at 30°C without denaturation, we digested proteins with protease and analyzed the resultant peptides by peptide mass fingerprinting.

The results showed that proteins electroblotted at 30°C still yielded normal peptide mass fingerprints. We also found that proteins electroblotted onto a DLC plate at 30°C can interact with other proteins and that the binding activity of the interacted proteins is maintained at 30°C.

CONCLUSION

To investigate the optimal temperature for efficient, effective electroblotting, we developed a semidry blotting apparatus that can regulate blotting temperatures, ranging from 4 to 45°C (±1°C).

Our results demonstrated that a high and reproducible electroblotting efficiency is not obtained at a low temperature, but at the relatively high temperature of 30°C. Furthermore, blotting performed at 30°C did not impede protein identification or the analysis of protein-protein interactions using MS.

ACKNOWLEDGEMENTS

We are grateful to Toyo Kohan Co., Ltd. for providing the DLC plate. This work was supported by Cooperation for Innovative Technology and Advanced Research in Evolutional Area (City Area).

REFERENCES

1) Figeys D, Pinto D. Proteomics on a chip: promising developments. Electrophoresis 2001;22:208–216.
2) Templin MF, Stoll D, Schwenk JM, Potz O, Kramer S, Joos TO. Protein microarrays: promising tools for proteomic research. Proteomics 2003;3:2155–2166.
3) Schweitzer B, Predki P, Snyder M. Microarrays to characterize protein interactions on a whole-proteome scale. Proteomics 2003;3:2190–2199.
4) Lueking A, Possling A, Huber O, Beveridge A, Horn M, Eickhoff H, Schuchardt J, Lehrach H, Cahill DJ. A nonredundant human protein chip for antibody screening and serum profiling. Mol Cell Proteomics 2003;2:1342–1349.
5) Iwafune Y, Tan JZ, Ino Y, Okayama A, Ishigaki S, Saito K, Suzuki N, Arima M, Oba M, Kamei S, Tanga M, Okada T, Hirano H. High-throughput on-chip identification and interaction analysis of gel-resolved proteins. The 56th Japanese Electrophoresis Society Symposium 2006;10.
6) Aisenberg S, Chabot R. Ion-beam deposition of thin films of diamondlike carbon. J Appl Phys 1971;42:2953–2957.
7) Laemmli UK. Cleavage of structural proteins during the assembly of the head of bacteriophage. Nature 1970; 227:680–685.

RESEARCH ARTICLE

Proteomic search for potential diagnostic markers and therapeutic targets for ovarian clear cell adenocarcinoma

Atsushi Morita[1, 2], *Etsuko Miyagi*[3], *Hidetaro Yasumitsu*[1], *Hiroshi Kawasaki*[1], *Hisashi Hirano*[1] *and Fumiki Hirahara*[3]

[1] International Graduate School of Arts and Sciences, Yokohama City University, Yokohama, Japan
[2] Discovery Research Laboratories, Shionogi, Osaka, Japan
[3] Department of Obstetrics and Gynecology, Yokohama City University School of Medicine, Yokohama, Japan

Received: September 30, 2005
Revised: July 9, 2006
Accepted: July 16, 2006

Clear cell adenocarcinoma (CCA) has a highly malignant potential in human epithelial ovarian cancer. The serum CA-125 is widely used as a marker for ovarian cancer, but the level is relatively low in CCA. Therefore, new sensitive biomarkers are required. In this report, we describe a promising proteomic analysis that is differentially expressed in CCA when compared to mucinous adenocarcinoma, using the ovarian cultured cell lines OVISE, OVTOKO, and MCAS. The disease-associated proteins were identified by 2-D differential gel electrophoresis (2-D DIGE) and MS. In this analysis, 18 up-regulated and 31 down-regulated spots were observed that had at least two-fold differences in the two CCA cell lines than in MCAS as control cells. Some of the proteins differentially expressed in CCA were previously observed as alternative expression levels in ovarian and/or other cancers in clinical samples. In a subsequent preliminary differential study using surgical specimens from patients with CCA, it was demonstrated that the identified proteins were expressed differentially in actual tissues, as well as in the CCA culture cells. The results from this investigation show the potentiality of a proteomic approach for identifying disease-associated proteins, which may eventually serve as diagnostic markers or therapeutic targets in CCA.

Keywords:
Biomarker / Ovarian cancer / Two-dimensional difference gel electrophoresis

1 Introduction

Ovarian and uterine cancers are the leading causes of death among gynecological malignancies, and the incidence rate of ovarian cancer tends to increase in some developed countries, including Japan [1–3]. It is widely recognized that a key point for successful clinical treatment is to diagnose the ovarian cancer at an early stage, and choose drugs that are appropriate for the histological type. Among the various types of human ovarian cancer, clear cell adenocarcinoma (CCA) is one with a highly malignant potential. Patients with CCA can be distinguished from those with other types of epithelial ovarian cancer as follows: (i) the recurrence rate is higher even in early stages; (ii) the 3 and 5-year survival rates for patients are significantly lower; and (iii) the response rate to platinum-based chemotherapy is lower [4]. In order to detect CCA and other types of ovarian cancer, the serum level of CA-125 is commonly used as the most available diagnostic marker. However, there are questions regarding its specificity and its ability to detect early stages because the level is elevated by other cancers [5], and also may be associated with various unrelated conditions such as pregnancy, endome-

Correspondence: Dr. Etsuko Miyagi, Department of Obstetrics and Gynecology, Yokohama City University School of Medicine, 3–9Fukuura, Kanazawa-ku, Yokohama 236–0004, Japan
E-mail: emiyagi@med.yokohama-cu.ac.jp
Fax: +81-45-701-3536

Abbreviations: BVA, biological variation analysis; **Cy**, cyanine fluorescent dye; **CCA**, clear cell adenocarcinoma, **EF-2**, elongation factor 2